

Testing flatness of the universe with probes of cosmic distances and growth

Michael J. Mortonson^{1,2,*}

¹*Department of Physics, University of Chicago, Chicago IL 60637*

²*Kavli Institute for Cosmological Physics and Enrico Fermi Institute,
University of Chicago, Chicago IL 60637, U.S.A.*

(Dated: November 8, 2018)

When using distance measurements to probe spatial curvature, the geometric degeneracy between curvature and dark energy in the distance–redshift relation typically requires either making strong assumptions about the dark energy evolution or sacrificing precision in a more model-independent approach. Measurements of the redshift evolution of the linear growth of perturbations can break the geometric degeneracy, providing curvature constraints that are both precise and model-independent. Future supernova, CMB, and cluster data have the potential to measure the curvature with an accuracy of $\sigma(\Omega_K) = 0.002$, without specifying a particular dark energy phenomenology. In combination with distance measurements, the evolution of the growth function at low redshifts provides the strongest curvature constraint if the high-redshift universe is well approximated as being purely matter dominated. However, in the presence of early dark energy or massive neutrinos, the precision in curvature is reduced due to additional degeneracies, and precise normalization of the growth function relative to recombination is important for obtaining accurate constraints. Curvature limits from distances and growth compare favorably to other approaches to curvature estimation proposed in the literature, providing either greater accuracy or greater freedom from dark energy modeling assumptions, and are complementary due to the use of independent data sets. Model-independent estimates of curvature are critical for both testing inflation and obtaining unbiased constraints on dark energy parameters.

I. INTRODUCTION

Cosmological measurements of the average spatial curvature of the spacetime metric are one of only a handful of methods available for testing the inflationary paradigm for the early universe. Current observations are consistent with the inflationary prediction of a nearly flat universe. However, the precision of curvature measurements is only at the percent level at best (e.g., [1, 2]), whereas the expected level of curvature in standard inflationary scenarios is generally much smaller. Moreover, obtaining the most precise limits on curvature requires assuming a particular simple form for the dark energy evolution due to the well-known “geometric degeneracy” between curvature and dark energy [3, 4, 5, 6, 7, 8, 9, 10, 11, 12, 13, 14, 15, 16, 17, 18, 19, 20, 21]. Inferences about inflation based on such curvature constraints are only valid if the assumed dark energy behavior is an adequate description of the true evolution.

Just as uncertainty about the dark energy evolution affects estimates of curvature, uncertainty about curvature limits our ability to constrain parameters of dark energy models with cosmic distances. One often assumes spatial flatness motivated by the predictions of inflation when constraining dark energy models, but the resulting parameter estimates may be biased if the true spatial curvature deviates even slightly from zero [3, 11, 13, 14, 15].

A few methods for using measured distances to obtain curvature estimates that are *independent* of the dark en-

ergy evolution have been proposed for use with future data sets. For example, Bernstein [18] proposed a technique using weak lensing galaxy–shear correlations to measure triangles of distances between the lensing and source galaxy planes and the observer, resulting in a curvature estimate that depends only on the assumed form of the spacetime metric. An alternate method by Knox [19] uses precisely measured distances at high redshift ($z \gtrsim 3$) combined with the distance to recombination from cosmic microwave background (CMB) data to infer the curvature without dependence on the low-redshift dark energy evolution.

In this work, we describe a different approach to model-independent curvature estimates that uses combinations of data sets that probe the distance–redshift relation and the growth of linear perturbations. The geometric degeneracy in distance data arises because distances depend on both the expansion rate (and therefore the dark energy evolution) and the spatial curvature. The growth of structure, on the other hand, depends only on the expansion rate. If one can measure both distances and growth over a similar range of redshifts, then constraints on the expansion rate from growth data can be used to break the degeneracy in distance data, providing a model-independent determination of the curvature. The only assumptions required are that general relativity (GR) is the correct theory of gravity governing the growth of structure and that dark energy does not cluster significantly on the scales of interest.

In Section II, we review the basic distance and growth relations and observables. Section III describes the geometric degeneracy in distances and how this degeneracy is broken by growth information. We then present fore-

*Electronic address: mjmort@uchicago.edu

casts for curvature constraints from future distance and growth data, beginning with descriptions of two methods of relating growth evolution on linear scales to an observed distance–redshift relation. The first, in Sec. IV, is based on a numerical exploration of general dark energy models carried out in Ref. [22] by Mortonson, Hu, and Huterer (hereafter, MHH09). The second method involves rewriting the equations for distances and growth so that the common dependence on the expansion rate drops out. The basis of this method of reconstructing the growth history from observed distances comes from Alam, Sahni, and Starobinsky [23], and in Sec. V, we summarize this work and extend it in several ways to allow the method to be applied to curvature forecasts. These two methods are complementary in several ways; the MCMC approach is more straightforward in terms of error propagation and the solution for the growth evolution, but it can be quite time-consuming and depends more on one’s priors on the dark energy evolution compared with the analytic growth reconstruction approach. The growth reconstruction method is therefore a useful tool for exploring the curvature-dependent relation between distances and growth for a variety of different cosmologies and assumed data sets, while the MCMC results help in testing and calibrating the analytic method and in providing accurate error estimates. Using both of these methods, forecasts for curvature from a combination of future supernova (SN), CMB, and X-ray cluster data are presented in Sec. VI. Finally, Sec. VII contains a summary and discussion of the results of this work.

II. PRELIMINARIES

A. Spatial curvature

Given that the universe appears to be spatially homogeneous and isotropic on large scales, the background metric can be written in the Friedmann-Robertson-Walker (FRW) form:

$$ds^2 = -dt^2 + a^2 \left[\frac{dD^2}{1 + \Omega_K H_0^2 D^2} + D^2 (d\theta^2 + \sin^2 \theta d\phi^2) \right], \quad (1)$$

which describes an expanding (or contracting) universe with scale factor $a(t)$, where D is the comoving radial coordinate and H_0 is the Hubble constant. The FRW metric has constant spatial curvature parametrized by Ω_K , where a flat universe has $\Omega_K = 0$, an open universe $\Omega_K > 0$, and a closed universe $\Omega_K < 0$. The curvature parameter is related to the total density of the components of the universe in units of the critical density for flatness, $\Omega_{\text{tot}} = \rho_{\text{tot}}/\rho_{\text{cr},0}$, by $\Omega_K = 1 - \Omega_{\text{tot}}$, where all densities are evaluated at the present time.

Theories of inflation predict that the universe is nearly flat ($\Omega_K \approx 0$), and the fact that current observations are consistent with flatness is viewed as supporting evidence

for inflation. The expected deviations from flatness are typically at or below the level of the initial curvature perturbations at the end of inflation, $|\Omega_K| \lesssim 10^{-5}$ (e.g., [24, 25]). The ultimate precision with which the curvature may be determined from observations is limited by cosmic variance and model selection considerations to $\sigma(\Omega_K) \sim 10^{-5} - 10^{-4}$ [26, 27]. While there are some theories of inflation in which the present value of the curvature is large enough to be potentially observable without excessive fine tuning of the initial conditions of inflation [25, 28, 29, 30, 31, 32, 33, 34, 35, 36, 37], a detection of nonzero curvature would challenge at least the simplest inflationary theories.

The strongest observational bounds on curvature are presently at the percent level, i.e. $\sigma(\Omega_K) \sim 0.01$. The main limits on curvature come from measurements of angular diameter distances in the CMB at $z \sim 1000$ and BAO at $z < 1$. However, these constraints rely on assuming a simple model for the dark energy such as a cosmological constant. More precise and more model-independent measurements of the spatial curvature would provide valuable tests of theories of inflation.

B. Distances

In a flat universe, the comoving distance D_f to an object at redshift z obtained by integrating over the comoving radial coordinate in the FRW metric is

$$D_f(z) = \int_0^z \frac{dz'}{H(z')}. \quad (2)$$

More generally, for universes with nonzero spatial curvature the comoving distance is

$$D(z) = \frac{1}{\kappa} S_K [\kappa D_f(z)], \quad (3)$$

where $\kappa \equiv (|\Omega_K| H_0^2)^{1/2}$ is the inverse of the curvature radius of the universe, and $S_K(x) = x$ for a flat universe, $\sinh x$ for an open universe, and $\sin x$ for a closed universe. Distances therefore depend on both the expansion rate, $H(z)$, and geometry, Ω_K . The distances at low redshifts for three models with varying spatial curvature are plotted in Fig. 1. Note that the curvature dependence is very weak at low redshifts, but high-redshift distances, e.g. the distance to recombination, are more sensitive to the geometry of the universe.

The main probes of distances we will consider here are Type Ia supernovae (SNe), standardizable candles whose average magnitudes are related to distances as

$$m(z) = 5 \log[H_0 d_L(z)] + \mathcal{M}, \quad (4)$$

where $\mathcal{M} = M - 5 \log(H_0/\text{Mpc}^{-1}) + 25$ combines the unknown absolute magnitude of the supernovae M and Hubble constant H_0 , both of which only affect the overall normalization of the SN distance–redshift relation. Since it involves unknown parameters that do not affect the

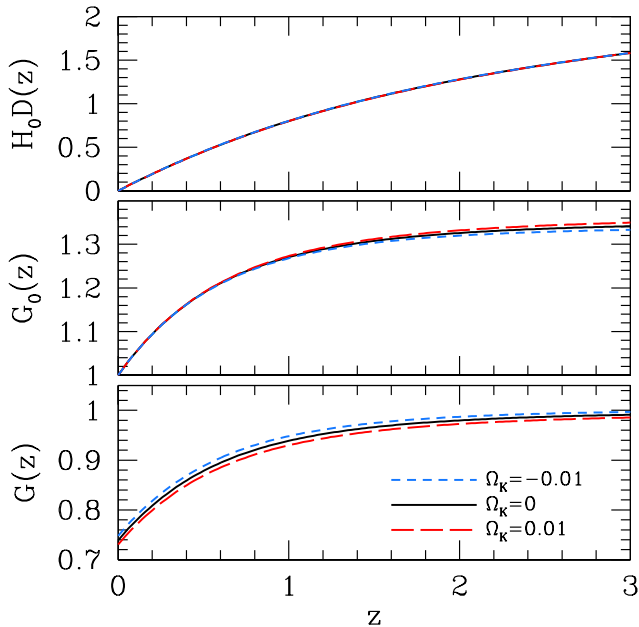


FIG. 1: Comoving distance (*top*), growth relative to $z = 0$ (*middle*), and growth relative to recombination (*bottom*) vs. redshift for flat, open, and closed models. For all three models, $\Omega_m = 0.24$ and $h = 0.73$. In the top panel, the 3 curves are indistinguishable in $H_0 D(z)$.

measured evolution of distances with redshift, \mathcal{M} is a “nuisance” parameter that is generally marginalized in a cosmological analysis of SN data.

Because the distance normalization is unknown, SN data determine relative distances, but not the absolute scale of the distance–redshift relation. However, SNe at low z can constrain the normalization since $\lim_{z \rightarrow 0} H_0 D(z) = z$ under reasonable assumptions about the evolution of $H(z)$ in the recent past.¹ Then for low-redshift SNe, the average magnitude from Eq. (4) is $m(z) \approx 5 \log z + \mathcal{M}$ which provides an estimate of \mathcal{M} .

We will also consider the angular diameter distance constraint from the acoustic scale of the CMB. The main effects of dark energy and curvature on the CMB enter through the distance to recombination at $z_* \approx 1089$ [38] and the matter density $\Omega_m h^2$, which affect the angular scale and amplitude of the acoustic peaks [20]. Dark energy and curvature also affect the large-scale CMB anisotropies through the integrated Sachs-Wolfe effect, but the information available is limited due to cosmic variance on those scales and the resulting constraints are relatively weak. We will therefore neglect this information in the curvature forecasts.

¹ For example, assuming that there was not a sudden large transition in the dark energy equation of state at $z \lesssim 0.01$ (e.g., see MHH09.)

Angular diameter distances can also be determined by measuring baryon acoustic oscillations in the matter power spectrum in the plane transverse to the line of sight. BAO can be a powerful probe of absolute distances, but incomplete redshift coverage and the need for wide redshift bins make the technique less suitable than Type Ia SNe as a primary source of the distance information for predictions of the growth evolution. However, BAO data can provide complementary constraints on curvature through other means (e.g., [19]).

C. Growth of linear perturbations

The growth of linear matter perturbations obeys

$$\ddot{\delta} + 2H\dot{\delta} - 4\pi G_N \rho_m \delta = 0 \quad (5)$$

where $\delta \equiv \delta\rho_m/\rho_m$ and overdots are derivatives with respect to time t . We assume here and throughout this work that general relativity is valid and that the dark energy is smooth on the relevant scales so that additional terms in the growth equation describing the clustering of dark energy can be neglected.

Equation (5) can be written in terms of $G \propto (1+z)\delta$ as

$$\begin{aligned} \frac{d^2 G}{d \ln a} + \left(4 + \frac{d \ln H}{d \ln a}\right) \frac{dG}{d \ln a} \\ + \left[3 + \frac{d \ln H}{d \ln a} - \frac{3}{2} \Omega_m(z)\right] G = 0, \end{aligned} \quad (6)$$

where $\Omega_m(z) = \Omega_m H_0^2 (1+z)^3 / H^2(z)$. The growth variable G is constant in a universe that contains only matter, so it is nearly constant at high redshifts during matter domination. We normalize the growth functions to $\delta(z=0) = 1$ and $G(z \rightarrow \infty) = 1$ so that

$$(1+z)\delta(z) = \frac{G(z)}{G(z=0)} \equiv G_0(z). \quad (7)$$

Figure 1 shows $G_0(z)$ and $G(z)$ for three models with different values of the spatial curvature.

From Eqs. (3) and (6) one can see that distances depend on both the expansion rate and geometry, while growth depends only on the expansion rate (and $\Omega_m H_0^2$ which is well determined by CMB data). Combinations of distance and growth information with similar redshift coverage therefore determine the geometry of the universe with reduced dependence on the expansion rate.

Measurements of cluster abundances in a range of redshift bins can probe the growth evolution at low redshifts, determining $G_0(z)$. Clusters can also constrain $G(z=0)$ to probe high-redshift changes in the growth evolution due to massive neutrinos or early dark energy by comparing the growth determined by low- z clusters with the predicted growth extrapolated to low redshifts from measurements of the CMB power spectrum amplitude at $z \sim 1000$ (e.g., see [39]). Ref. [40] contains current examples of both types of measurements using an X-ray cluster sample.

Assuming that dark matter halos of mass M host galaxy clusters with the same mass, the cluster abundance depends on cosmology primarily through the halo mass function dn/dM and the comoving volume element in a solid element $d\Omega$ and redshift slice dz ,

$$\frac{dV}{d\Omega dz} = \frac{D^2(z)}{H(z)}. \quad (8)$$

The mass function describing the comoving density of dark matter halos of mass M at redshift z can be written as

$$\frac{dn}{dM} = \frac{\Omega_m \rho_{\text{cr},0}}{M} \frac{d \ln \sigma^{-1}(M, z)}{dM} f(\sigma(M, z)). \quad (9)$$

Here $\sigma^2(M, z)$ is the variance of linear matter density perturbations,

$$\sigma^2(M, z) = \left[\frac{G_0(z)}{1+z} \right]^2 \int d \ln k \Delta^2(k) W^2(kR(M)), \quad (10)$$

where $R(M) = [3M/(4\pi\Omega_m\rho_{\text{cr},0})]^{1/3}$, $\Delta^2(k)$ is the dimensionless power spectrum of linear matter perturbations at $z = 0$ with comoving wavenumber k , and $W(kR) = 3j_1(kR)/kR$ is the Fourier transform of a spherical top-hat window function with radius R .

The function $f(\sigma)$ in Eq. (9) parametrizes the mass function in a way that is relatively independent of redshift and cosmological parameters. The dependence on σ is exponential as $\sigma \rightarrow 0$, and since $\sigma(M, z) \propto G_0(z)$, the abundance of massive clusters is exponentially sensitive to the growth function.

Additional details about the cluster abundance can be found in Sec. VID, where we describe the dependence of curvature estimates from SN, CMB, and cluster data on the modeling of the cluster growth information.

D. Expansion rate

The Friedmann equation gives the expansion rate as determined by the evolution of the density of various components:

$$H(z) = H_0 \left[\Omega_m(1+z)^3 + \Omega_r(1+z)^4 + \frac{\rho_{\text{DE}}(z)}{\rho_{\text{cr},0}} + \Omega_K(1+z)^2 \right]^{1/2}, \quad (11)$$

where ρ_{DE} is the dark energy density and Ω_m , Ω_r , and Ω_K are the present matter density, radiation density, and effective curvature density, respectively, in units of the critical density. Here we generalize the dark energy phenomenology to allow arbitrary evolution of the dark energy density. For a general time-dependent dark energy equation of state $w(z)$, the dark energy density evolves as

$$\rho_{\text{DE}}(z) = \rho_{\text{cr},0} \Omega_{\text{DE}} \exp \left[3 \int_0^z dz' \frac{1+w(z')}{1+z'} \right], \quad (12)$$

where $\Omega_{\text{DE}} = 1 - \Omega_m - \Omega_r - \Omega_K$ is the present fraction of dark energy.

The data we consider for curvature forecasts only have the ability to constrain the detailed dark energy evolution at low redshifts ($z < z_{\text{max}}$ where $z_{\text{max}} \sim 1.5$), so we only allow complete freedom in $\rho_{\text{DE}}(z)$ at late times. In models with $w(z) \sim -1$, the dark energy fraction decreases rapidly with increasing redshift and therefore the exact form of the high-redshift dark energy evolution is unimportant; for example, for flat Λ CDM, $\Omega_{\text{DE}}(z_*) \sim 10^{-9}$. However, models have been proposed in which the dark energy remains a significant fraction of the total density even at high z , such as scalar field models that track the density of the dominant matter and radiation components at early times [41, 42, 43]. To account for such possibilities, we parametrize early dark energy using an effective constant equation of state

$$w(z > z_{\text{max}}) = w_\infty, \quad (13)$$

as in MHH09. At $z > z_{\text{max}}$, the dark energy density is

$$\rho_{\text{DE}}(z) = \rho_{\text{DE}}(z_{\text{max}}) \left(\frac{1+z}{1+z_{\text{max}}} \right)^{3(1+w_\infty)}. \quad (14)$$

Although this may not be a realistic model for early dark energy, it should be sufficient to absorb at least small effects of early dark energy on curvature estimates. Dark energy that behaves like a cosmological constant at $z > z_{\text{max}}$ would have $w_\infty = -1$ and tracking models have $w_\infty = 0$. Other values of w_∞ may provide an effective description of other types of models, e.g. tracking models that transition to $w < 0$ at $z \gg z_{\text{max}}$ can be approximated by a constant equation of state in the range $-1 < w_\infty < 0$. We examine how well this approach works in the context of different early dark energy models (as well as models with massive neutrinos, which have effects that are indistinguishable below the neutrino free streaming scale from early dark energy in the observables considered here) in Sec. VIB.

Since w_∞ only specifies the redshift evolution of the dark energy density at $z > z_{\text{max}}$ but not its normalization, the density at some redshift is required to completely describe the early dark energy model. It is convenient to use the fraction of dark energy at z_{max} , $\Omega_{\text{DE}}(z_{\text{max}})$, for this purpose. One way to estimate this quantity from SN data is to differentiate $D_f(z)$ at z_{max} , since from Eqs. (2) and (11) we can obtain

$$\frac{\rho_{\text{DE}}(z_{\text{max}})}{\rho_{\text{cr},0}} = E_{\text{max}}^2 - \sum_{i \neq \text{DE}} \Omega_i (1+z_{\text{max}})^{3(1+w_i)}, \quad (15)$$

where $E_{\text{max}} = H(z_{\text{max}})/H_0 = H_0^{-1}(\partial z/\partial D_f)|_{z=z_{\text{max}}}$.

E. Data for forecasts

In this section, we summarize the main data assumptions we use for the curvature forecasts presented in Sec. VI. These data include future Type Ia supernova and CMB observations as probes of distances, and X-ray cluster abundances as a probe of the linear growth history. The characteristics of the former set of distance data match those assumed in MHH09.

The supernova sample is taken to match the planned redshift distribution for the SuperNova/Acceleration Probe (SNAP) [44], which covers redshifts $0.1 < z < 1.7$. In addition, we assume a sample of 300 low-redshift SNe at $0.03 < z < 0.1$. The intrinsic SN magnitude dispersion is taken to be $\sigma_{\text{stat}} = 0.15$, and the systematic error is modeled as $\sigma_{\text{sys}} = 0.02[(1+z)/2.7]$ in redshift bins of width $\Delta z = 0.1$. Then the uncertainty in relative distances from SNe in a $\Delta z = 0.1$ bin with N SNe is

$$\sigma_{\ln H_0 D} = 0.2 \ln 10 \sqrt{N^{-1} \sigma_{\text{stat}}^2 + \sigma_{\text{sys}}^2}. \quad (16)$$

The CMB distance priors we use are modeled on the specifications for the recently-launched Planck satellite [45]. As in MHH09, we describe the CMB data with a 2D Fisher matrix F^{CMB} including the distance to recombination, $D(z_*)$, and the physical matter density, $\Omega_m h^2$. The elements of the covariance matrix $C^{\text{CMB}} = (F^{\text{CMB}})^{-1}$ are $C_{xx}^{\text{CMB}} = (0.0018)^2$, $C_{yy}^{\text{CMB}} = (0.0011)^2$, and $C_{xy}^{\text{CMB}} = -(0.0014)^2$, where $x = \ln[D(z_*)/\text{Mpc}]$ and $y = \Omega_m h^2$.

In addition to the distance constraints from SN and CMB data, in some cases we will consider the effect of additional priors. For the MCMC analysis, we use the priors of MHH09 which correspond to constraints from currently available data, including an 11% H_0 prior from HST Key Project data [46], a 3.7% BAO measurement of $D(z = 0.35)$ from SDSS [2], and a 2.5% upper limit on the fraction of early dark energy at recombination from the WMAP temperature angular power spectrum [47]. For the growth reconstruction forecasts, we also consider future priors including a 1% measurement of H_0 [48] and a 1% upper limit on the dark energy fraction at recombination from CMB data, $\Omega_{\text{DE}}(z_*)$. A stronger limit of $\sim 0.2\%$ on the early dark energy fraction may be obtainable with future observations of CMB lensing in the context of specific parametrizations of early dark energy [49, 50], but here we adopt a more conservative prior to allow for the possibility that the limit may weaken upon including more general early dark energy behavior.

Each of these constraints supplementing the SNAP and Planck data is implemented as a Gaussian prior with mean equal to the value in the fiducial cosmology. We will see in Sec. VI that for a variety of cosmological models, particularly those in which the deviations in the high-redshift density evolution from the concordance model are mild, these additional priors are unnecessary for curvature estimates from future distance and growth data sets.

For growth forecasts, we consider constraints on the

amplitude and redshift evolution of galaxy cluster abundances using observations from the proposed International X-ray Observatory (IXO) [51]. The IXO is projected to obtain 1–2% measurements of the growth function $G_0(z)$ in $\Delta z = 0.1$ bins over $0 < z < 2$, assuming that distances and the expansion rate are effectively fixed by other data sets such as SNe. When combined with the expected 1% measurement by Planck of the amplitude of scalar fluctuations from the CMB power spectra, the X-ray cluster data should also provide a $\sim 1 - 2\%$ measurement of $G(z)$ at $z < 2$.

We approximate the cluster growth information from IXO (and Planck for comparison of the cluster abundance and CMB power spectrum amplitudes) by a Gaussian likelihood with uniform uncertainties in $G_0(z)$ at $z \leq z_{\text{max}}$ in $\Delta z = 0.1$ bins and $G(z_{\text{max}})$, using $z_{\text{max}} = 1.5$ corresponding to the maximum redshift at which distances are well constrained by SNe. Our forecasts in Sec. VI assume optimistic 1% growth uncertainties from IXO as the default assumption, but in Sec. VID we also examine how curvature constraints weaken for more pessimistic assumptions and consider how degeneracies between distances and growth in the cluster observables may affect the predicted curvature constraints.

III. THE GEOMETRIC DEGENERACY

In this section, we present examples of the degeneracy between curvature and dark energy evolution in the distance–redshift relation, and show how growth information can break this degeneracy.

The geometric degeneracy can take a variety of forms, depending on the dark energy modeling and the available data. For example, even for a cosmological constant Λ there is a degeneracy between Ω_Λ and Ω_K if the only input is the distance to recombination from the CMB (e.g., [7, 8, 9]). Adding more data breaks the degeneracy for the cosmological constant model, but the degeneracy persists for more complex dark energy models. Taken to an extreme, even if one has exact measurements of the distance–redshift relation over the entire history of the universe, there is still a degeneracy if we allow arbitrary evolution of the dark energy density with redshift. This general form of the geometric degeneracy is what we focus on here.

The degeneracy in distance data is apparent if we differentiate Eq. (3) and use Eq. (11) to solve for the dark energy density:

$$\frac{\rho_{\text{DE}}(z)}{\rho_{\text{cr},0}} = \frac{1 + \Omega_K [H_0^{\text{fid}} D^{\text{fid}}(z)]_{\text{SN}}^2}{(\partial [H_0^{\text{fid}} D^{\text{fid}}(z)]_{\text{SN}} / \partial z)^2} - \sum_{i \neq \text{DE}} \Omega_i (1+z)^{3(1+w_i)}, \quad (17)$$

assuming that SN data provide relative distance measures $[H_0^{\text{fid}} D^{\text{fid}}(z)]_{\text{SN}}$ for some fiducial cosmology. [Note that this generalizes Eq. (15).] Thus for any value of the

spatial curvature, there exists some dark energy evolution that matches a given set of distance measurements.

The ability of dark energy to match distances for any value of Ω_K is weakened if we introduce some mild restrictions on the dark energy evolution, for example requiring that the dark energy density be nonnegative. Observational constraints beyond the distance–redshift relation can also limit the possible dark energy behavior; for example, a dark energy fraction of a few percent or more at recombination would distort the CMB temperature power spectrum in ways that are not observed in WMAP data [5, 47, 52].

In practice, however, the redshift coverage of data is limited, so degenerate cosmological models only need to match distances at the redshifts where we can actually measure distances. Within the redshift “gaps” in our observations, the dark energy evolution can deviate from Eq. (17) and still satisfy all available observational constraints.

Figure 2 shows the dark energy fraction, distance, and growth of four example models chosen to illustrate these points. These models all have nonzero curvature (two open and two closed), but Ω_m , h , and w_∞ are adjusted so that they all match relative SN distances $H_0 D(z)$ at $z < z_{\max}$ with $z_{\max} = 1.7$ (see middle panel of Fig. 2) and CMB constraints on $D(z_*)$ and $\Omega_m h^2$ for a flat Λ CDM model with $\Omega_m = 0.24$ and $h = 0.73$.

For each model, a dotted line shows how the dark energy evolution would extend to $z > z_{\max}$ if we required the models to match $H_0 D(z)$ at all distances in the range $0 < z < z_*$ (but not the CMB absolute distance); for the closed models this would require a negative dark energy density, $\Omega_{\text{DE}}(z) < 0$, at high z , and for the open models $\Omega_{\text{DE}}(z_*) \sim 10 - 20\%$ which violates current CMB constraints. However, due to the lack of observational constraints at $z_{\max} < z < z_*$, not only can we find models with nonzero curvature that match the SN and CMB data of the fiducial flat Λ CDM model, but there is in fact a set of degenerate models for each value of Ω_K with different combinations of the matter density and early dark energy parameters.

Specifically, to match an observed distance to recombination $[D^{\text{fid}}(z_*)]_{\text{CMB}}$ as well as SN distances, the constraint that these models must satisfy [in addition to Eq. (17) at $z < z_{\max}$] is

$$\begin{aligned} \kappa \int_{z_{\max}}^{z_*} \frac{dz}{H(z)} &= S_K^{-1} \{ \kappa [D^{\text{fid}}(z_{\max})]_{\text{CMB}} \} \\ &- S_K^{-1} \{ \kappa H_0^{-1} [H_0^{\text{fid}} D^{\text{fid}}(z_*)]_{\text{SN}} \}. \end{aligned} \quad (18)$$

The bottom panel of Fig. 2 shows that despite being degenerate in the SN and CMB distance data, these models are distinct in their growth evolution for different values of the spatial curvature. This separation based on curvature is mostly independent of the $\{\Omega_m, w_\infty\}$ values. This indicates that growth observations can break the degeneracy between Ω_K , Ω_m , and w_∞ that is present in SN and CMB data and provide model-independent information about the curvature.

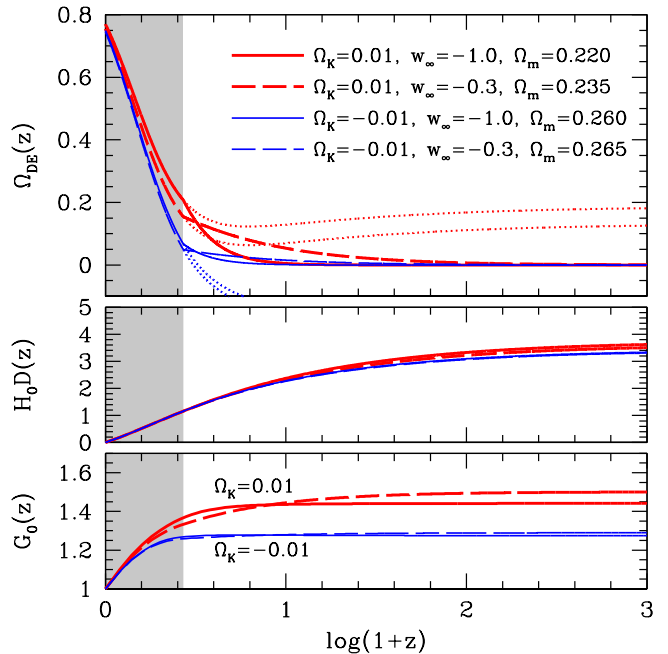


FIG. 2: Geometric distance degeneracy between curvature and dark energy dynamics. Curves show the dark energy fraction (*top panel*), relative distances (*middle panel*), and growth relative to $z = 0$ (*bottom panel*) for models with distance–redshift relations that are degenerate with a fiducial flat Λ CDM model with $\Omega_m = 0.24$ and $h = 0.73$. Thick red curves correspond to open models with $\Omega_K = 0.01$, and thin blue curves are closed models with $\Omega_K = -0.01$. The solid and dashed curves only match the relative distances at $z < 1.7$ (*shaded region*) and the CMB distance at $z \sim 1000$, but not distances at intermediate redshifts where the dark energy equation of state is assumed to be constant, $w(1.7 < z < z_*) = w_\infty$. Dotted curves in the top panel show the dark energy evolution that would be required to match relative distances of the fiducial model at *all* redshifts. Parameters of each model are given in the top panel legend; for each model, h is set so that $\Omega_m h^2$ is the same as in the fiducial model.

Note that a precise independent measurement of H_0 (or, equivalently, combinations of SN relative distances with absolute distances, e.g. from BAO) determines the value of Ω_m since the CMB precisely constrains $\Omega_m h^2$. This removes one parameter from the degeneracy described above, so the remaining degeneracy is between curvature and dark energy only with the matter density fixed. The freedom to match observations for any value of Ω_K is thereby reduced, leading to constraints on curvature even in the absence of growth information. We discuss these constraints in relation to the curvature estimates from distances and growth in Sec. VI.

IV. MCMC METHOD

For both the MCMC analysis presented in this section and the growth reconstruction method (Sec. V), it is convenient to view the constraints on curvature from distances and growth in the following way. First, we assume that the distance–redshift relation is precisely measured at low z by SNe and at high z by the CMB. Given this distance data and assuming the validity of GR, we can use either the MCMC likelihood analysis or the analytic growth reconstruction technique to compute a *predicted* growth history that is consistent with the measured distances. The main sources of uncertainty in the relation between measured distances and predicted growth are curvature and early dark energy (or massive neutrinos), with curvature primarily affecting the growth relative to $z = 0$ [$G_0(z)$] and early dark energy affecting the growth relative to high z [$G(z)$] (MHH09). Because of this dependence, *measurements* of $G_0(z)$ yield constraints on curvature when they are compared with the predicted growth history, and measurements of $G(z)$ help constrain deviations from matter domination at high z .

Computing the distances and growth functions for each MCMC sample of the cosmological parameter space is straightforward as it only requires using Eqs. (2) and (3) to obtain the distance–redshift relation and solving Eq. (6) for the growth. We will see in Sec. V that the growth reconstruction scheme is somewhat more complicated to implement.

One of the main advantages of using the MCMC approach is that the estimation of parameter uncertainties is also straightforward: as long as the MCMC samples have converged to a stationary distribution approximating the joint posterior probability of the parameters (Sec. IV A), the marginalized probability for curvature can be obtained by binning the samples based on the value of Ω_K . However, the parameter chains sometimes converge quite slowly, especially for very general parametrizations of dark energy combined with curvature. External priors like those described in Sec. II E can improve MCMC convergence in some cases.

A drawback of the MCMC analysis is that although we are trying to obtain model-independent results, we must still specify some model for the dark energy evolution. To provide a general parametrization at low z , we use several principal components of the dark energy equation of state as described in the following section. However, there is still some degree of unavoidable dependence on dark energy priors. In the absence of strong growth constraints, the choice of priors can influence the curvature constraints as we will see in Sec. VI. The growth reconstruction method of Sec. V does not require specifying a parametrization for the dark energy equation of state and therefore suffers less from such effects.

A. Growth predictions from distances

The MCMC method of predicting the linear growth of perturbations is based on computing the growth functions of a large sample of cosmological models that fit observed distances well. The range of growth functions spanned by these models constitutes a prediction for the growth evolution based on distances. This procedure is described in detail by MHH09, and here we present a summary.

Two main ingredients are required: a parametrization of cosmological models and a description of how well these models fit the observed distances. Since we are concerned about possible degeneracies between dark energy and curvature, we want to allow a wide variety of dark energy behavior. This is accomplished using a basis of principal components (PCs) for the dark energy equation of state $w(z)$ to parametrize general dark energy evolution below a redshift z_{\max} :

$$w(z) - w_{\text{fid}}(z) = \sum_i \alpha_i e_i(z), \quad (19)$$

where the PCs are ordered according to how well they are measured by a particular combination of data. The PCs are eigenvectors of the Fisher matrix for the distance data, taken here and in MHH09 to be the SNAP SN sample, CMB distance data from Planck, and current priors on H_0 , $D(z = 0.35)$, and $\Omega_{\text{DE}}(z_*)$ as described in Sec. II E. Figure 3 shows the redshift dependence of the 15 lowest-variance PCs.

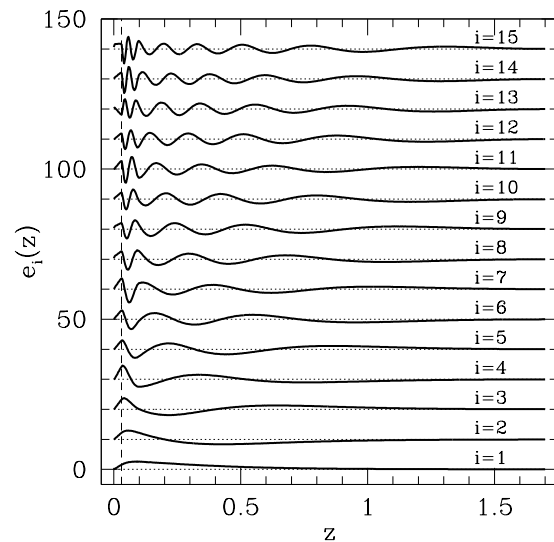


FIG. 3: The first 15 principal components of $w(z)$ for SNAP and Planck (increasing variance from bottom to top), with 500 redshift bins between $z = 0$ and $z_{\max} = 1.7$ and $w_{\text{fid}} = -1$. The vertical dashed line shows the minimum redshift of the data assumed for computing the PCs, $z_{\min}^{\text{SN}} = 0.03$. The PCs are offset vertically from each other for clarity with dotted lines showing the zero point for each component.

The Fisher matrix for the PCs is computed at some fiducial dark energy model specified by the equation of state $w_{\text{fid}}(z)$, usually taken to be a cosmological constant. The redshift range of the PCs is the same as the range of the SN data, with maximum redshift $z_{\text{max}} = 1.7$. The PCs are normalized as

$$\sum_{i=1}^{N_{z,\text{PC}}} [e_i(z_j)]^2 = \sum_{j=1}^{N_{z,\text{PC}}} [e_i(z_j)]^2 = N_{z,\text{PC}}, \quad (20)$$

where $N_{z,\text{PC}}$ is the number of redshift bins, so that the shapes of the PCs are roughly independent of the chosen bin width.

The highest-variance principal components have a negligible effect on observable distances and growth due to their rapid oscillation in redshift. We therefore truncate the sum in Eq. (19) at 15 PCs, found by MHH09 to be a sufficient number for a complete representation of the effects of dark energy variation at $z < z_{\text{max}}$ on the distance and growth observables. The dark energy description is completed by specifying the high-redshift evolution through the constant effective equation of state $w(z > z_{\text{max}}) = w_{\infty}$. Besides varying w_{∞} and the $w(z)$ PC amplitudes in the MCMC analysis, we also include Ω_{m} , H_0 (parametrized through the combination $\Omega_{\text{m}}h^2$), and Ω_{K} as MCMC parameters, so there are 19 parameters in all.

Using top-hat priors on the PC amplitudes, one can restrict the value of $w(z)$ to a particular range, conservatively erring on the side of allowing too many models rather than too few. The priors corresponding to the range $w_{\text{min}} < w < w_{\text{max}}$ are $\alpha_i^{(-)} \leq \alpha_i \leq \alpha_i^{(+)}$, where

$$\alpha_i^{(\pm)} \equiv \frac{1}{2N_{z,\text{PC}}} \sum_{j=1}^{N_{z,\text{PC}}} [(w_{\text{min}} + w_{\text{max}} - 2w_{\text{fid}})e_i(z_j) \pm (w_{\text{max}} - w_{\text{min}})|e_i(z_j)|], \quad (21)$$

assuming constant $w_{\text{fid}}(z)$ (MHH09).² For example, requiring $-1 \leq w \leq 1$ for quintessence models places strong limits on the allowed PC amplitudes. In the interest of keeping the dark energy evolution as general as possible, here we will only consider the weakest priors on w used in MHH09 corresponding to $-5 \leq w \leq 3$.

By varying the cosmological parameters, computing the likelihood of each model for the assumed distance data sets, and using the Metropolis-Hastings criterion for deciding whether or not to accept a proposed step in the parameter space, the resulting set of parameter combinations trace out the joint posterior probability of the parameters (e.g., [54, 55, 56]). To determine when the number of MCMC samples is large enough that the parameter chains have converged to the posterior distribution, we run 4 independent chains and require that the

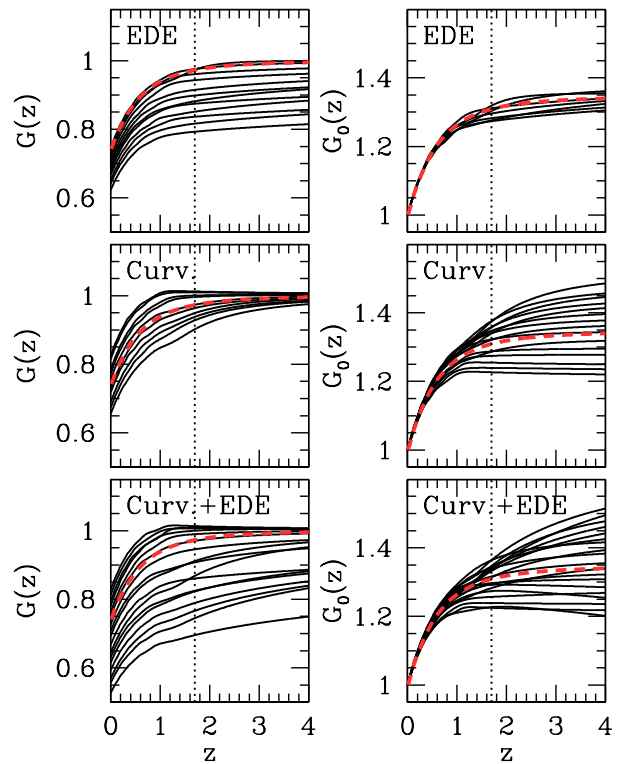


FIG. 4: Growth functions of MCMC samples with general dark energy equation of state variations at $z < 1.7$ within the range $-5 \leq w \leq 3$, including either early dark energy (EDE) at $z > 1.7$ ($w_{\infty} \neq -1$; *top*), curvature ($\Omega_{\text{K}} \neq 0$; *middle*), or both (*bottom*). The left panels show growth relative to early times, and the right panels show growth relative to the present. Dashed red curves show growth in the fiducial flat Λ CDM model ($\Omega_{\text{m}} = 0.24$, $h = 0.73$). Samples are selected randomly from those with likelihoods satisfying $\Delta\chi^2 \leq 4$, but for visual clarity we plot samples that are approximately evenly spaced in $G(z=0)$ (*left*) or $G_0(z=4)$ (*right*). The dotted vertical line in each panel marks the division between the low- z and high- z dark energy descriptions at $z = 1.7$.

Gelman-Rubin statistic satisfy $R - 1 \lesssim 0.01$, indicating that the variance of the mean value of a parameter between different chains is much smaller than the variance within a single chain [57].

This MCMC procedure produces a variety of cosmological models that fit the fiducial distance data reasonably well. For each of these models, we compute the growth history using Eq. (6). The distribution of the resulting growth functions then forms the prediction for growth from distances.

Plotting sets of predicted growth functions from MCMC analyses with different degrees of freedom in the cosmological models reveals how distance-matched growth functions depend on curvature and early dark energy. Figure 4 shows the growth evolution of selected MCMC samples in chains with early dark energy varying and curvature fixed to $\Omega_{\text{K}} = 0$, curvature varying

² Similar top-hat priors are derived in Ref. [53] in the context of principal components of the reionization history.

and early dark energy fixed to $w_\infty = -1$, or variation in both curvature and early dark energy (in addition to variation in the low- z dark energy equation of state via principal components). Early dark energy mainly affects the growth amplitude relative to high redshift, $G(z)$, with very little effect on the shape of the growth evolution at low z characterized by $G_0(z)$. On the other hand, curvature strongly influences $G_0(z)$ but has less of an effect on $G(z)$: for a fixed distance–redshift relation, open (closed) models have larger (smaller) $G_0(z)$ than a flat universe. This is the same effect that we see in the geometric degeneracy examples in Fig. 2.

This difference between the effects of curvature and early dark energy supports the claim that measurements of $G_0(z)$, combined with distance measurements, can constrain curvature with little dependence on early dark energy or other high-redshift phenomena. Measurements of $G(z)$ can be used to place limits on any residual effects that early dark energy might have on these curvature estimates.

One interesting feature of the spread of the distance-matched $G_0(z)$ evolution due to curvature is that it tells us how precise growth measurements must be to improve on model-independent curvature constraints. In particular, for the forecasts shown here, the uncertainty in the predicted growth at $z \sim 1$ (at 68% CL) is about 5–10% (MHH09),³ so any direct measurements of the growth evolution that are less precise than this will not appreciably reduce the uncertainty in Ω_K . For example, current cluster measurements of growth are not yet precise enough to significantly reduce the uncertainty in curvature from current distance constraints [40].

As observed in MHH09, MCMC estimates of Ω_K from distance data are dependent on $w(z)$ priors if “phantom” dark energy models ($w < -1$) are allowed. This dependence is essentially a volume effect related to the large volume of degenerate $w < -1$ models that are correlated with $\Omega_K < 0$ [58]. Precise growth measurements help reduce this dependence on dark energy priors as we will see in Sec. VI.

B. MCMC estimates of curvature

The procedure described in the previous section produces chains of parameter combinations that match the SN and CMB distance data, as well as the additional priors. To obtain forecasts for Ω_K from distance and growth data, we need to add the growth information from measured cluster abundances.

The first step for including the growth constraints is

to simply compute the growth evolution for each MCMC sample. With a growth history associated with each distance-matched MCMC sample, we then use importance sampling of the parameter chains [59] to reweight the samples according to the growth likelihood described in Sec. II E. The posterior probability for Ω_K from the distance and growth forecasts is then computed as usual by marginalizing over the other MCMC parameters. In Sec. VI, we will describe the resulting curvature constraints and compare them with the forecasts from the growth reconstruction method.

V. GROWTH RECONSTRUCTION

The MCMC approach in the previous section used a general parametrization of the dark energy equation of state to predict growth evolution from measured distances by searching for $w(z)$ satisfying the distance constraints and computing the corresponding growth evolution. However, it is possible to go from distances to growth directly without using an intermediary like $w(z)$. Here we will first summarize this growth reconstruction method and then show how it can be used to study model-independent curvature constraints. Additional details about the procedure we use for growth reconstruction from simulated SN and CMB data are provided in Appendix B.

The growth reconstruction equations derived by Alam, Sahni, and Starobinsky [23, 60] express the amplitude of linear perturbations δ as a function of the comoving distance assuming spatial flatness, D_f [Eq. (2)]. For convenience, we define a dimensionless comoving distance, $\chi \equiv H_0 D_f$.⁴

Starting from Eq. (5) for the linear growth function, we can rewrite the equation in terms of χ by using $d/dt = -H_0(1+z)d/d\chi$ and writing the matter density as $\rho_m = 3\Omega_m H_0^2 / (8\pi G_N)(1+z)^3$ to get

$$H_0^2(1+z)[(1+z)\delta']' - 2H_0H(1+z)\delta' - \frac{3}{2}H_0^2\Omega_m(1+z)^3\delta = 0, \quad (22)$$

where primes denote derivatives with respect to χ . Since $d\chi/dz = H_0/H$, we can replace H by $H_0 dz/d\chi = H_0(1+z)'$. After dividing by $H_0^2(1+z)^3$, this yields

$$\frac{[(1+z)\delta']' - 2(1+z)'\delta'}{(1+z)^2} = \frac{3}{2}\Omega_m\delta. \quad (23)$$

The left hand side of this equation is equal to $[(1+z)\delta'' - (1+z)'\delta']/(1+z)^2$, which can be written as

$$\left(\frac{\delta'}{1+z}\right)' = \frac{3}{2}\Omega_m\delta. \quad (24)$$

³ Note that the uncertainty in growth predictions depends on the priors assumed in addition to the SN and CMB data forecasts, in this case taken from current H_0 , BAO, and CMB data as described in Sec. II E.

⁴ Note that in Ref. [23] this quantity is called E , but here we use the notation χ instead to avoid confusion with the common definition $E(z) = H(z)/H_0$.

Integrating Eq. (24) over χ leads to the main growth reconstruction equation [23, 60], which is an integral equation for $\delta(\chi)$:

$$\delta(\chi) = 1 + \delta'_0 \int_0^\chi d\chi_1 [1 + z(\chi_1)] + \frac{3}{2} \Omega_m \int_0^\chi d\chi_1 [1 + z(\chi_1)] \int_0^{\chi_1} d\chi_2 \delta(\chi_2), \quad (25)$$

where δ'_0 is the derivative of $\delta(\chi)$ at $z = 0$, and the growth function is normalized to $\delta(z = 0) = 1$. Solving for the growth function involves making an initial guess for $\delta(\chi)$ and plugging it into the right hand side of Eq. (25), taking the resulting $\delta(\chi)$ from the left hand side and plugging it back in to the right hand side, and repeating until the solution has converged.

As noted in Ref. [23], Eq. (25) only requires integration of observed quantities, so the growth reconstruction method is more stable to the presence of scatter in the data than other methods that use derivatives of the observed distance–redshift relation. Differentiation uses information from the data over only a small range of redshift or χ , whereas an integral from 0 to χ uses data over the entire range which helps average out statistical noise. For χ near 0 the number of data points used is still small, but the reduced statistical power can be offset by having smaller intrinsic uncertainties at lower redshifts.

By differentiating Eq. (25) and evaluating it at $\chi = \chi(z_{\max})$, we can shift the boundary condition on the derivative of $\delta(\chi)$ from $z = 0$ to $z = z_{\max}$:

$$\delta'_0 = \frac{\delta'_{\max}}{1 + z_{\max}} - \frac{3}{2} \Omega_m \int_0^{\chi(z_{\max})} d\chi \delta(\chi), \quad (26)$$

where $\delta'_{\max} = \delta'(\chi(z_{\max}))$. Then Eq. (25) can be rewritten as

$$\delta(\chi) = 1 + \frac{\delta'_{\max}}{1 + z_{\max}} \int_0^\chi d\chi_1 [1 + z(\chi_1)] - \frac{3}{2} \Omega_m \int_0^\chi d\chi_1 [1 + z(\chi_1)] \int_{\chi_1}^{\chi(z_{\max})} d\chi_2 \delta(\chi_2). \quad (27)$$

This is the form of the growth reconstruction equation that we will use for the curvature forecasts.

One advantage of setting the boundary condition for $\delta'(\chi)$ at $\chi(z_{\max})$ instead of $\chi = 0$ is that δ'_{\max} depends mainly on the assumed cosmology at high redshifts, whereas δ'_0 depends on not only the high- z assumptions but also the low- z SN data constraints and iterative growth solution. Also, setting δ'_{\max} makes it easier to ensure that $\delta(\chi)$ is smooth at $\chi(z_{\max})$ by requiring the same derivative there for both the fiducial model at $z > z_{\max}$ and the reconstructed growth function at $z < z_{\max}$. Rather than setting the value of the $\delta'(\chi)$ boundary condition using an integral over $\delta(\chi)$ as suggested in Ref. [60], here we use an approximate analytic form for the high-redshift growth function valid when matter is the dominant component.

Solving Eq. (27) for $\delta(\chi)$ requires specifying the function $z(\chi)$ and three parameters: Ω_K , Ω_m , and δ'_{\max} . Some of these inputs to the growth reconstruction are set by the SN and CMB data constraints, while others are free parameters. Because of this link between the distance data sets and the growth reconstruction, some of the scatter in the SN and CMB observations will propagate to uncertainties in the reconstructed growth. We compute the mean values of reconstructed growth observables and their uncertainties using Monte Carlo simulations of the SN and CMB data, modeled on SNAP and Planck as for the MCMC method.

The following steps summarize the procedure for these Monte Carlo simulations. Additional details about each step are provided in Appendix B.

1. Assume values for the curvature and any additional parameters describing the high-redshift cosmology; here we use w_∞ for parametrizing early dark energy. The output of the Monte Carlo simulations will be the conditional probability for the growth observables given Ω_K and w_∞ .
2. Draw a realization of the SN data $[H_0 D(z)]$ for the fiducial cosmology and estimate $z(\chi)$ from the data. Given an assumed value of Ω_K , we can invert Eq. (3) to get

$$\chi(z) = \frac{1}{\sqrt{|\Omega_K|}} S_K^{-1} \left[\sqrt{|\Omega_K|} H_0 D(z) \right], \quad (28)$$

where $S_K^{-1}(x)$ is $\sinh^{-1} x$ for an open universe, $\sin^{-1} x$ for a closed universe, and x if $\Omega_K = 0$. To reduce bias in the estimated $\chi(z)$ relation, we take the maximum redshift for the growth reconstruction to be $z_{\max} = 1.5$, slightly lower than the maximum SN redshift of $z = 1.7$ that was used as z_{\max} in the MCMC method of Sec. IV (see Appendix B for details).

3. Draw a realization of the CMB data $[D(z_*)$ and $\Omega_m h^2]$ and use Eq. (18) along with the assumed values of Ω_K and w_∞ to compute the value of Ω_m required by the CMB parameters.
4. Steps 1–3 fix the cosmological model at $z > z_{\max}$, so we can compute $G(z_{\max})$ for this cosmology as one of the growth observables, and use the approximate high- z growth solution of Appendix A [Eq. (A5)] to set δ'_{\max} for the growth reconstruction.
5. Solve Eq. (27) to find the reconstructed growth, $\delta(\chi)$, for the particular realization of SN and CMB data. Use the $\chi(z)$ relation from step 2 to express this solution as $\delta(z)$ or $G_0(z)$.

Repeating these steps for many realizations of the distance data produces a distribution of the growth observables \mathbf{g} , which include $G(z_{\max})$ from step 4 and $G_0(z)$

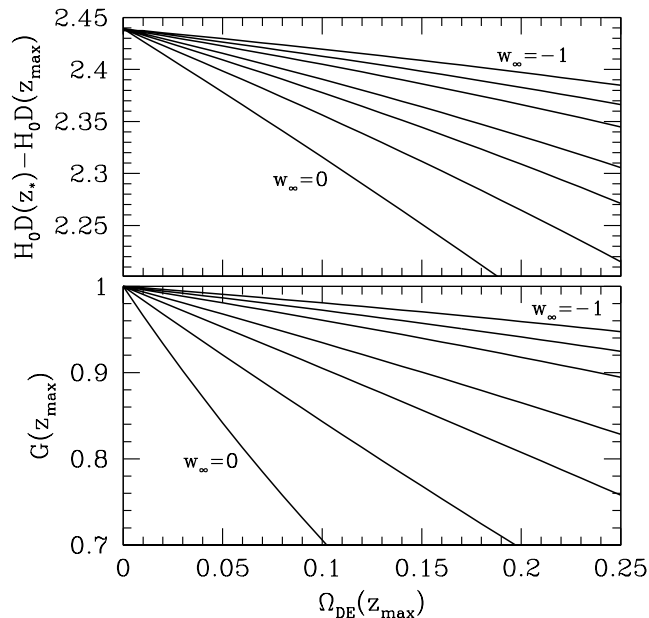


FIG. 5: Effect of early dark energy on distance and growth. *Top panel:* Difference between the distance to recombination and the distance to $z_{\max} = 1.5$. *Bottom panel:* Growth at z_{\max} relative to recombination. Early dark energy models are parametrized by the fraction of dark energy at z_{\max} and $w_{\infty} = w(z > z_{\max})$. From top to bottom in each panel, $w_{\infty} = -1, -0.7, -0.5, -0.3, -0.2, -0.1$, and 0. Flat Λ CDM is assumed here with $\Omega_m = 0.24$ and $h = 0.73$.

from step 5, for the chosen values of Ω_K and w_{∞} . This procedure can be carried out at several different values of Ω_K and w_{∞} to map out the conditional probability $P(\mathbf{g}|\Omega_K, w_{\infty})$. This probability describes the growth predictions from distance data in the context of the growth reconstruction method.

Note that in step 3, there will generally be degeneracies between Ω_K , Ω_m , and early dark energy in the CMB constraints, increasing the uncertainty in the model-independent estimate of curvature. Fortunately, measurements of growth relative to high z can reduce this uncertainty. The top panel of Figure 5 shows the effect of various early dark energy models on the difference between the distance to recombination and the distance to z_{\max} . Both $w_{\infty} > -1$ and $\Omega_{\text{DE}}(z_{\max}) \gtrsim 0.05$ are required for the distances to be significantly affected. As the bottom panel of Fig. 5 shows, the growth relative to high redshift, $G(z_{\max})$, is sensitive to early dark energy in a way that is similar to how the distances depend on early dark energy. Therefore, precise measurement of the growth at z_{\max} relative to growth at early times (for example, by comparing the normalization of growth from cluster abundances with the amplitude of CMB power spectra) can constrain the effect of early dark energy on high- z distances, thereby reducing the uncertainty in the Ω_m - Ω_K relation from the CMB constraints. Although $G(z)$ predicted from distances is relatively insensitive to

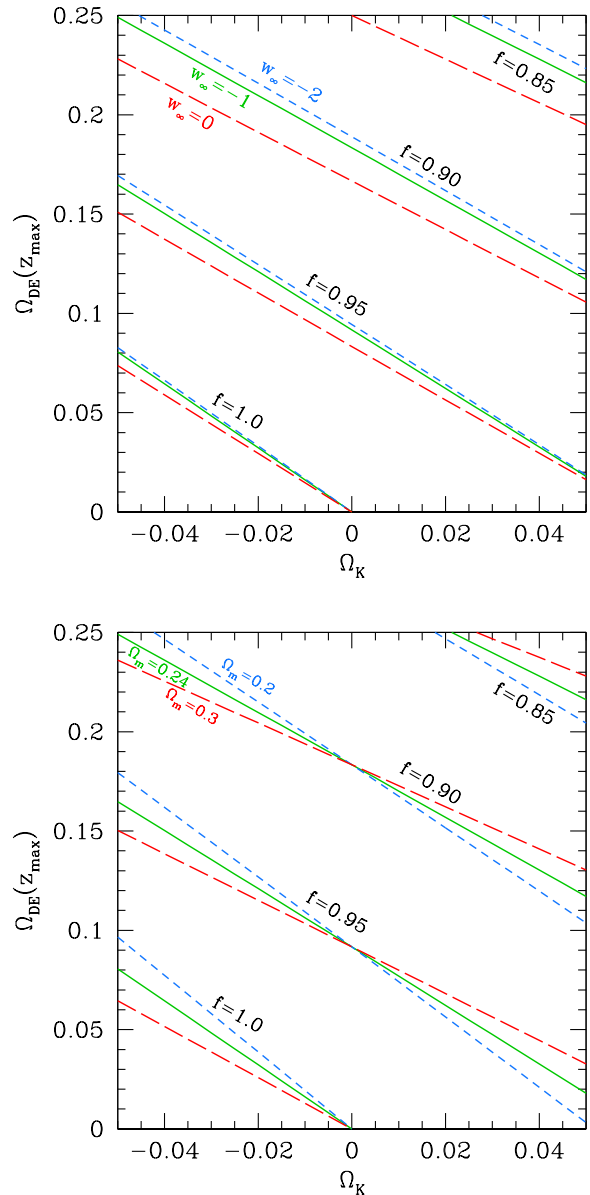


FIG. 6: Contours of the growth rate f at $z_{\max} = 1.5$ as a function of Ω_K and $\Omega_{\text{DE}}(z_{\max})$, for three choices of w_{∞} at fixed $\Omega_m = 0.24$ (*top*) and three choices of Ω_m at fixed $w_{\infty} = -1$ (*bottom*).

curvature in a direct sense (see Fig. 4), it provides an important complementary constraint to the curvature estimates from distances and $G_0(z)$ that reduces model dependence.

The approximation for δ'_{\max} used in step 4, which is described in Appendix A, assumes that the curvature and early dark energy fractions at high z are small enough that the growth can be written as a perturbation to the matter-dominated solution where $G(z)$ is constant. The dependence of δ'_{\max} on early dark energy turns out to be fairly weak. Figure 6 shows the value

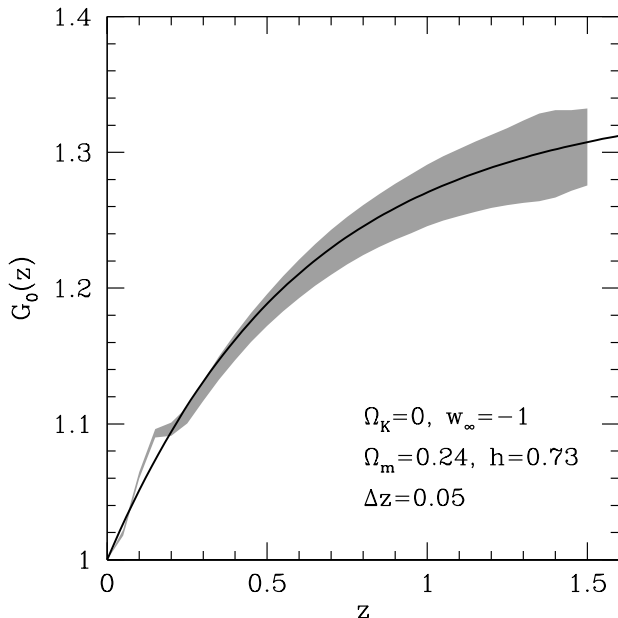


FIG. 7: Growth reconstruction for $\Omega_K = 0$ and $w_\infty = -1$ where the fiducial cosmology is flat Λ CDM with $\Omega_m = 0.24$ and $h = 0.73$. The shaded band is the 68% CL region for $G_0(z)$ reconstructed from simulated SNAP and Planck data, and the true growth evolution is plotted as a solid curve. The redshift bin width for the reconstruction is $\Delta z = 0.05$.

of the growth rate $f = d \ln \delta / d \ln a = 1 + d \ln G / d \ln a$ at z_{\max} as a function of curvature and the fraction of dark energy at z_{\max} . Changing w_∞ only slightly shifts the contours of f , especially for models that satisfy CMB constraints on the dark energy fraction at recombination. Therefore, at fixed curvature $\delta'_{\max} / \delta(z_{\max}) = -(1 + z_{\max})^{-1} E(z_{\max}) f(z_{\max})$ mainly depends on $\Omega_{\text{DE}}(z_{\max})$, which can be estimated from the SN data using Eq. (15). Likewise, for curvature at the level of a few percent or less, uncertainty in Ω_m does not strongly affect δ'_{\max} .

In summary, the growth reconstruction method as outlined above requires choosing values for two parameters: the curvature Ω_K and the early dark energy equation of state w_∞ . All other quantities are estimated from the distance information provided by measurements of SNe and the CMB. Given this distance data, the end result of the growth reconstruction procedure is a prediction for the growth evolution for each $\{\Omega_K, w_\infty\}$ pair, $P_d(\mathbf{g}|\Omega_K, w_\infty)$.

Figure 7 shows an example of the reconstructed growth evolution from the distance data for the fiducial flat Λ CDM model, assuming $\Omega_K = 0$ and $w_\infty = -1$. In the lowest redshift bins, the growth reconstruction is biased due to the relatively small number of SNe in the SNAP distribution at low z , but over most of the redshift range the reconstruction is in good agreement with the true growth function.

A. Growth reconstruction estimates of curvature

By combining the predicted growth from distances $P_d(\mathbf{g}|\Omega_K)$ with measurements of the growth observables \mathbf{g} , we can obtain an estimate of Ω_K from the growth reconstruction method.⁵

$$P(\Omega_K) = \int d\mathbf{g} P_d(\Omega_K, \mathbf{g}) P_g(\mathbf{g}), \quad (29)$$

where $P_d(\Omega_K, \mathbf{g}) = P_d(\mathbf{g}|\Omega_K) P_{\text{prior}}(\Omega_K)$ is the joint probability for curvature and growth observables from the growth reconstruction from distance data as described in the previous section combined with any additional prior information about Ω_K , and $P_g(\mathbf{g})$ represents the constraints on the growth observables from probes of the growth history such as clusters. We use subscripts d and g to indicate constraints coming from distance and growth data, respectively.

Assuming that the Monte Carlo simulations produce conditional probabilities for growth observables at fixed Ω_K that can be approximated as a multivariate Gaussian, we can write

$$P_d(\mathbf{g}|\Omega_K) = \frac{1}{(2\pi)^{n/2} (\det \mathbf{F}_d)^{-1/2}} \exp\left(-\frac{1}{2} \delta \mathbf{g}^T \mathbf{F}_d \delta \mathbf{g}\right), \quad (30)$$

where \mathbf{F}_d is the Fisher matrix for the n growth observables from the simulated distance data, computed by inverting the covariance matrix \mathbf{C}_d from the growth reconstruction Monte Carlo simulations, and $\delta \mathbf{g} \equiv \mathbf{g} - \bar{\mathbf{g}}_d$ is the deviation of the growth observables from the mean growth reconstruction solution. Note that both \mathbf{F}_d and $\bar{\mathbf{g}}_d$ depend on the value of Ω_K (and additional parameters such as w_∞).

If the growth observations are also well approximated by a multivariate Gaussian with covariance matrix \mathbf{C}_g , Fisher matrix $\mathbf{F}_g = \mathbf{C}_g^{-1}$, and mean values $\bar{\mathbf{g}}_g$ (assumed to be equal to the true growth history of the fiducial model), then the posterior probability for Ω_K in Eq. (29) is

$$P(\Omega_K) \propto P_{\text{prior}}(\Omega_K) [\det(\mathbf{I} + \mathbf{F}_d^{-1} \mathbf{F}_g)]^{-1/2} \times \exp\left[\frac{1}{2} \Delta^T \mathbf{F}_g (\mathbf{F}_d + \mathbf{F}_g)^{-1} \mathbf{F}_g \Delta - \frac{1}{2} \Delta^T \mathbf{F}_g \Delta\right], \quad (31)$$

where $\Delta \equiv \bar{\mathbf{g}}_d - \bar{\mathbf{g}}_g$ is the difference between the average growth evolution predicted from distances at a particular assumed value of Ω_K and the true growth evolution, and \mathbf{I} is the $n \times n$ identity matrix. We describe the resulting forecasts for curvature in the next section.

⁵ For notational compactness, in this section we suppress dependence on additional parameters varied in the growth reconstruction analysis such as w_∞ , but in general, these should appear along with Ω_K wherever there is dependence on curvature.

VI. MODEL-INDEPENDENT CURVATURE CONSTRAINTS

In this section, we use the techniques for combining distance and growth measurements described in Sections IV and V to obtain forecasts for spatial curvature constraints from the simulated SN, CMB, and cluster data of Sec. II E.

The accuracy of curvature estimates depends not only on the assumed characteristics of the distance and growth data sets, but also on the fiducial, “true” cosmological model assumed for the forecasts. We begin in Sec. VI A with the simple case in which the fiducial model is flat Λ CDM, and use this example to compare forecasts from the MCMC and growth reconstruction methods. In Sec. VI B, we generalize to other fiducial cosmologies that are more or less consistent with constraints from current data. Tests of the dependence of these results on modeling of the SN, CMB, and cluster data sets are described in Sections VI C and VI D. Finally, Sec. VI E compares these distance and growth constraints on curvature with other model-independent tests of curvature.

A. Flat Λ CDM

We begin by comparing MCMC and growth reconstruction constraints on Ω_K in the context of a flat Λ CDM fiducial cosmology, taking the parameters to be $\Omega_m = 0.24$ and $h = 0.73$. Figure 8 shows curvature forecasts for two different sets of data. Both cases include distance constraints from SNe modeled after SNAP and CMB data based on Planck. On their own, these data sets would place almost no limits on curvature, assuming that general forms of the dark energy evolution are allowed.

In the top panel of Fig. 8, the SN and CMB data are supplemented by weak priors based on current data: an 11% H_0 prior from HST Key Project data [46], a 3.7% BAO measurement of $D(z = 0.35)$ from SDSS [2], and a 2.5% upper limit on the fraction of early dark energy at recombination from the WMAP temperature spectrum [47]. We adopt these priors here for consistency with the MCMC analysis of model-independent growth predictions in MHH09.

Using only the current priors in addition to the SN and CMB data, curvature is determined with an accuracy of $\sigma(\Omega_K) \sim 0.02$. However, the results depend on the analysis method. In particular, the MCMC constraints on Ω_K depend strongly on the assumed priors on the dark energy parameters (MHH09). For priors that are flat in the $w(z)$ principal component amplitudes [$P(\alpha_i) = \text{constant}$], the curvature constraint is biased toward $\Omega_K < 0$. Taking alternate priors which are instead flat in the *density* associated with each principal component at $z_{\text{max}} = 1.7$,

$$\frac{\rho_i(z_{\text{max}})}{\rho_i(0)} = \exp \left[3\alpha_i \int_0^{z_{\text{max}}} dz \frac{e_i(z)}{1+z} \right], \quad (32)$$

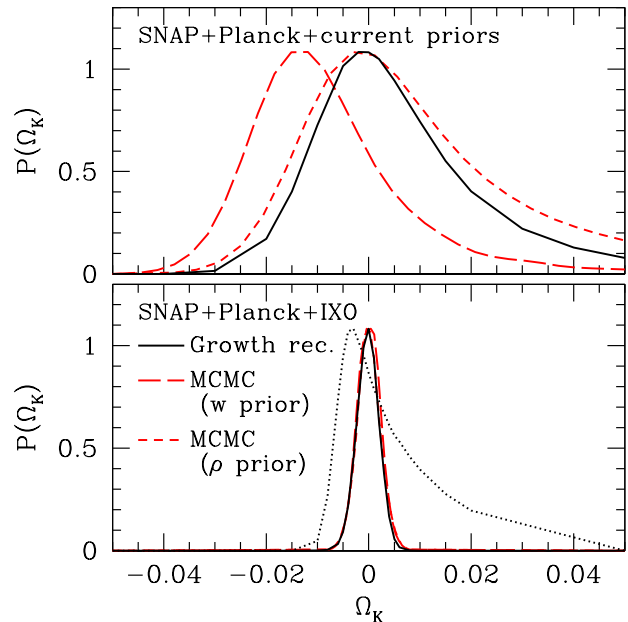


FIG. 8: Comparison of MCMC and growth reconstruction curvature forecasts for the flat Λ CDM fiducial cosmology. *Top panel:* combining *current* priors on H_0 , $D(z = 0.35)$, and $\Omega_{\text{DE}}(z_*)$ with SN and CMB forecasts based on SNAP and Planck, respectively. *Bottom panel:* combining SNAP and Planck forecasts with cluster forecasts based on IXO as a probe of the growth evolution. For comparison, the dotted curve shows a forecast for SNAP, Planck, and future 1% measurements of H_0 and $\Omega_{\text{DE}}(z_*)$ (without growth constraints).

the resulting curvature constraint is less biased, but has a long tail at $\Omega_K > 0$. The curvature estimate from the growth reconstruction method using the same data is more consistent with the flat-density prior constraint from the MCMC analysis, but has a slightly narrower distribution.

The lower panel of Fig. 8 shows the resulting curvature forecasts when we drop the current priors on H_0 , BAO distance, and the early dark energy fraction, and instead combine the SN and CMB distances with 1% growth function measurements from IXO clusters. Using growth to break the geometric degeneracy in distances, the curvature constraint improves to an accuracy of $\sigma(\Omega_K) = 0.0022$. Not only is this a much stronger constraint on curvature than without the growth information, but it is also significantly less dependent on the parameter estimation methodology. The MCMC constraints using different types of dark energy priors are consistent with each other and unbiased, and the forecast from growth reconstruction agrees with the MCMC results.

Since we are taking a forecast for future data as the source of growth information, it is not quite fair to compare this future distance plus growth constraint with the curvature estimate from *current* Hubble constant, BAO,

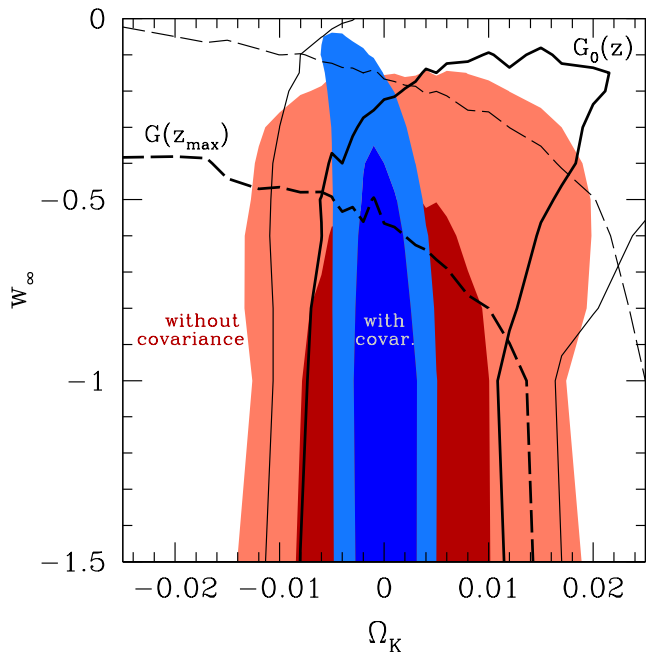


FIG. 9: Forecasts in the Ω_K - w_∞ plane for the flat Λ CDM fiducial model, including various combinations of growth information in addition to SN and CMB distance constraints: $G(z_{\max})$ (dashed contours), $G_0(z)$ at $z \leq 1.5$ (solid contours), or both (shaded blue contours). The combined growth constraint *without* the covariance between the predicted $G(z_{\max})$ and $G_0(z)$ from the growth reconstruction is shown as shaded red contours. Contours are plotted at 68% CL (thick curves/dark shading) and 95% CL (thin curves/light shading).

and early dark energy priors. We use those priors only to illustrate the possible dependence of estimates that do not use growth information on dark energy priors or other details of the analysis, and for comparison with the earlier MCMC results from MHH09. If we instead combine SNAP and Planck forecasts with *future* priors on H_0 and $\Omega_{\text{DE}}(z_*)$, both with 1% accuracy (see Sec. II E), the curvature estimate improves but remains weaker and more skewed than the distance plus growth forecasts (see bottom panel of Fig. 8). We discuss the impact of future BAO measurements and other types of data on model-independent curvature constraints in comparison to constraints from distances and growth in Sec. VI E.

The MCMC and growth reconstruction forecasts show that combinations of distances and growth have the potential to provide reliable, model-independent measurements of curvature with $\sim 0.2\%$ accuracy, at least in the context of a flat Λ CDM cosmology. Before exploring the forecasts for this method for other fiducial cosmological models, we examine how different parts of the distance and growth data contribute to the curvature estimate.

Figure 9 shows the impact of different components of the assumed growth information from IXO cluster data on the joint constraint on curvature and early dark en-

ergy. Recall from Sec. II E that there are two types of growth information used here: 1% measurements of the growth evolution at $0 < z < z_{\max}$ that probe $G_0(z)$, and a 1% measurement of the growth at z_{\max} relative to the growth at recombination, $G(z_{\max})$. The unshaded contours in Fig. 9 show the results of using each of these growth constraints separately (in addition to the SN and CMB data).

If the growth information consists only of $G_0(z)$ (i.e. just the relative evolution of the cluster mass function at low z with unknown normalization relative to the CMB), the constraints on Ω_K are a few times weaker than the combined growth constraints for $w_\infty \lesssim -1$. As w_∞ approaches 0, the G_0 constraint shifts toward open models. As a result, $P(\Omega_K)$ marginalized over w_∞ is weakened even further and is skewed toward $\Omega_K > 0$.

On the other hand, growth information from $G(z_{\max})$ only (e.g., comparing σ_8 from clusters and the CMB) places very weak constraints on curvature, only significantly limiting the range of allowed open models. However, the information provided by $G(z_{\max})$ is complementary to that from $G_0(z)$ since it cuts off the G_0 degeneracy at $\Omega_K > 0$ and $w_\infty \gtrsim -0.5$. By removing this degeneracy, the combined growth constraints are much less sensitive to the early dark energy parameters, resulting in a stronger, unbiased curvature estimate.

Moreover, the covariance between $G(z_{\max})$ and $G_0(z)$ predictions from measured distances reduces the curvature uncertainty beyond what would be expected from simply combining the separate $G(z_{\max})$ and $G_0(z)$ constraints. As shown in Fig. 9, the distance plus growth constraints on curvature with the $G(z_{\max}) - G_0(z)$ covariance removed by hand (red shaded contours) are a few times weaker than the full constraint including this covariance (blue shaded contours).

The covariance between the growth observables comes primarily from the CMB distance constraint. Matching the distance to recombination requires a balance between the low- z and high- z dark energy evolution. For example, increasing the dark energy density at low redshifts tends to decrease $D(z_*)$, and decreasing the high-redshift dark energy density can compensate for this shift. The CMB distance priors therefore anticorrelate the dark energy evolution at early and late times. This results in a positive correlation between the predicted values of $G_0(z)$ and $G(z_{\max})$ from SN and CMB data. In the example above, the larger dark energy density at low z enhances the suppression of the late-time growth of perturbations, which corresponds to higher values of $G_0(z)$. A smaller dark energy density at high z results in less growth suppression at early times and therefore a higher value of $G(z_{\max})$.

This positive correlation between G_0 and G for growth reconstructed from distances is the opposite of the effect of curvature. Relative to a flat universe, an open geometry tends to suppress growth at both early and late times while a closed geometry has the opposite effect. This means that increasing Ω_K increases $G_0(z)$ while de-

creasing $G(z_{\max})$, and vice versa. The positive covariance between these two types of growth observables required by CMB constraints therefore leads to stronger limits on curvature.

To summarize, in the case of flat Λ CDM the primary information about curvature from growth combined with distance data comes from $G_0(z)$, as expected based on the discussions in the previous sections. However, normalization of low-redshift growth relative to the high redshift of recombination can significantly improve the accuracy of the curvature estimate by reducing early dark energy uncertainties and through the covariance with the low- z growth evolution required to match SN and CMB distances.

B. Dependence on cosmology

We now turn to curvature forecasts from distances and growth for fiducial cosmologies other than the flat Λ CDM example of the previous section. Since the analytic growth reconstruction method is more efficient at exploring different assumptions about the true cosmology and properties of the data, we will primarily rely on that method for the forecasts in this section.

As the first test of dependence on the fiducial cosmology underlying the data, we consider flat Λ CDM models with different parameters from those in the previous section. For a model with $\Omega_m = 0.3$ and $h = 0.7$, the constraint on curvature is almost identical to that for $\Omega_m = 0.24$ and $h = 0.73$. Thus variation of flat Λ CDM parameters in the range allowed by current data does not significantly affect the curvature forecasts.

Next, we consider models with different values of the curvature. We saw in the previous section that if the universe is actually flat, future distance and growth probes can exclude at 95% CL alternate models with $|\Omega_K| \gtrsim 0.005$. It is also interesting to ask whether true nonzero curvature could be detected (i.e. distinguished from $\Omega_K = 0$) using this method. Figure 10 compares the forecast for the flat Λ CDM model of the previous section with forecasts for an open model and a closed model, both with $|\Omega_K| = 0.01$ and the other parameters unchanged. The resulting constraints on curvature for the open and closed models are nearly identical to that for the flat model, except for being shifted to be centered on the true curvature. Therefore, distances and growth from SNAP, Planck, and IXO data enable percent-level curvature to be cleanly distinguished from flatness.

Curvature forecasts are similarly precise and unbiased for models with different dark energy evolution from Λ CDM at low redshifts. For example, if we adopt the commonly-used parametrization of the dark energy equation of state $w(z) = w_0 + w_a z / (1 + z)$ [61, 62] with $w_0 = -0.8$ and $w_a = -0.5$, and keep all other parameters the same as in the fiducial flat Λ CDM model, then the growth reconstruction analysis again returns an unbiased estimate of Ω_K with $\sigma(\Omega_K) \approx 0.002$. Note that

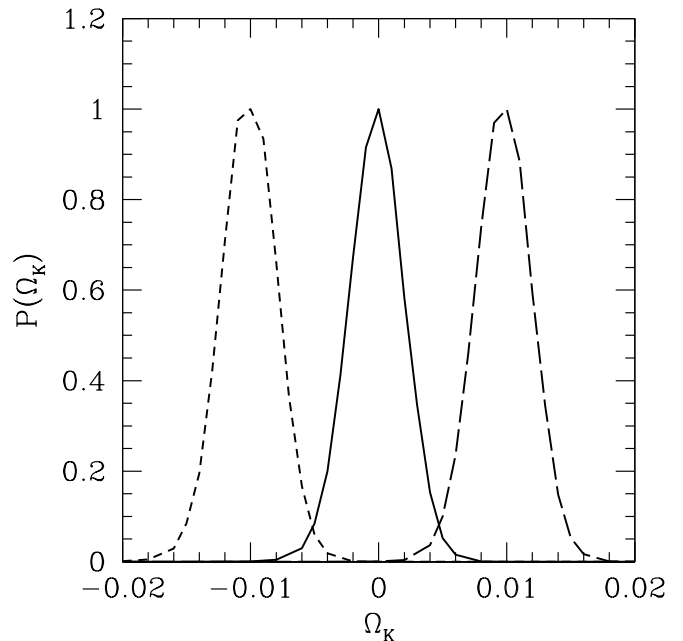


FIG. 10: Growth reconstruction forecast of the marginalized probability of Ω_K for models with $\Omega_K = 0$ (solid), $\Omega_K = -0.01$ (short dashed), and $\Omega_K = 0.01$ (long dashed). Each model is a Λ CDM cosmology with $\Omega_m = 0.24$ and $h = 0.73$.

in this model, dark energy is negligible at high redshifts since $\lim_{z \rightarrow \infty} w(z) = w_0 + w_a$ which is less than -1 .

Although changing parameter values in the context of flat Λ CDM and similar cosmological models has little effect on the accuracy of the estimated curvature from future distances and growth, changing the fiducial model for the high-redshift universe can have more interesting consequences. We consider first early dark energy scenarios and then models with massive neutrinos. In both cases, the $G(z_{\max})$ constraint takes on a much larger role and constraints from $G_0(z)$ alone become unreliable.

Given the fact that current data are consistent with flat Λ CDM, models with significant early dark energy are more likely to be open than flat or closed since the geometric effect of negative spatial curvature can compensate for the reduced distance to recombination due to early dark energy (e.g., [4]). Figure 11 shows the SNAP+Planck+IXO constraints on a $w_0 - w_a$ model with $w_0 + w_a \approx 0$ to act as early dark energy and $\Omega_K = 0.025$ compared with the flat Λ CDM model of the previous section.

For the open early dark energy model, the best fit to distance and growth constraints is near the true parameter values (the effective value of w at $z > z_{\max}$ that matches the fiducial CMB distance and growth function normalization is $w_\infty \approx -0.25$). However, a significant degeneracy between curvature and early dark energy remains even with the combination of distance and growth

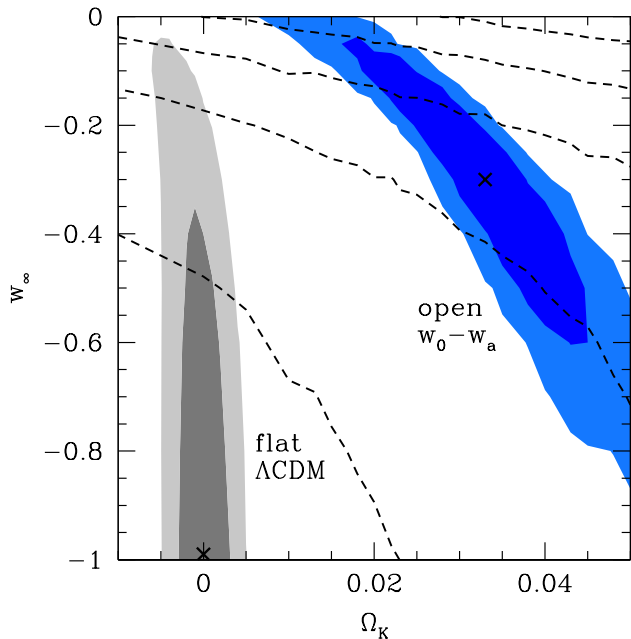


FIG. 11: Forecast in the $\Omega_K - w_\infty$ plane for an open universe with early dark energy: $\Omega_K = 0.025$, $w_0 = -1.08$, $w_a = 1.02$ (shaded blue contours, right). The mean value of $G(z_{\max})$ for the growth function reconstructed from the fiducial distances of this model is plotted with dashed, unshaded contours at $G(z_{\max}) = 0.5, 0.6, 0.7, 0.8$, and 0.9 , from top to bottom. The flat Λ CDM forecast from Fig. 11 is plotted for comparison (shaded gray contours, left). Crosses mark the best fit point for each model. Shaded contours are plotted at 68% and 95% CL.

data. One consequence of this is that the curvature constraints marginalized over w_∞ would be misleading; for example, the shape of the $w_0 - w_a$ model constraints in the $\Omega_K - w_\infty$ plane cause $P(\Omega_K)$ to be biased high, although maximizing the likelihood over w_∞ instead of marginalizing would reduce the apparent bias somewhat. Furthermore, the marginalized Ω_K constraints are weaker than the 0.2% flat Λ CDM estimate, despite the fact that the contours in the $\Omega_K - w_\infty$ plane are of comparable width.

Despite the loss of precision in the curvature estimates in the presence of early dark energy, the constraints from distances and growth for such models remain extremely interesting since they provide clear evidence for either large amounts of early dark energy or nonzero curvature, if not both. And, in fact, for models like this example with $\Omega_K \gtrsim 0.02$ it is still possible to confidently exclude a flat universe independent of the assumptions about early dark energy.

Unlike the models without early dark energy where the main curvature constraints come from distances plus $G_0(z)$, and $G(z_{\max})$ has a lesser role (see Fig. 9), for early dark energy models the $G(z_{\max})$ constraint combined with distance data is the main source of both the

early dark energy *and* curvature constraints. In fact, curvature estimates using distances and measurements of $G_0(z)$ alone would indicate a preference for flatness and no early dark energy even if the true model was the $w_0 - w_a$ example with $\Omega_K = 0.025$. Other types of curvature constraints, for example using a 1% H_0 prior in addition to SNAP and Planck data, similarly fail to detect the nonzero curvature and early dark energy for such models. While a measurement of $G(z_{\max})$ is a helpful additional constraint on models in which dark energy only becomes important at late times, it is crucial for obtaining accurate constraints on models with early dark energy. Figure 11 shows contours of $G(z_{\max})$ for the open $w_0 - w_a$ model; the forecast roughly follows these contours, but is tilted somewhat due to the $G_0(z) - G(z_{\max})$ covariance from the CMB distance constraint.

To test how well the early dark energy parametrization with w_∞ can model other forms of early dark energy evolution, we use the parametrization of Ref. [63] in which the dark energy fraction approaches a constant value Ω_e at high redshift:

$$\Omega_{\text{DE}}(a) = \frac{\Omega_{\text{DE}} - \Omega_e(1 - a^{-3w_0})}{\Omega_{\text{DE}} + \Omega_m a^{3w_0}} + \Omega_e(1 - a^{-3w_0}), \quad (33)$$

where $w_0 = w(z=0)$. (This form assumes $\Omega_K = 0$, so we only use it to simulate distance and growth data for a flat universe.) The equation of state at high redshifts during matter domination is $w \approx 0$. However, since the transition between $w \approx w_0$ at low z and $w \approx 0$ at high z can occur at $z \neq z_{\max}$ the effective value of w_∞ that best matches distance and growth observables for this model is not necessarily $w_\infty = 0$.

We take the parameters for the simulated SNAP, Planck, and IXO data to be $w_0 = -0.9$, $\Omega_e = 0.02$, $\Omega_m = 0.225$, $h = 0.73$, and $\Omega_K = 0$. As for the previous early dark energy example, the constraint on Ω_K marginalized over w_∞ is biased due to the shape of the likelihood in the $\Omega_K - w_\infty$ plane. However, for this model there is some additional bias such that the best fit is at $\Omega_K \approx 0.004$. Given the increased width of the likelihood in Ω_K [$\sigma(\Omega_K) \sim 0.003$] and the long tail toward $\Omega_K < 0$, the true curvature $\Omega_K = 0$ is not strongly disfavored despite this bias. The bias in Ω_K is likely a reflection of the limitations of the w_∞ parametrization of early dark energy, suggesting that a more flexible parametrization may be needed to accurately model a wide variety of early dark energy behavior.

Additional priors can help reduce bias in curvature even with the default w_∞ modeling of early dark energy in the growth reconstruction analysis. The open models favored in the analysis of the Doran & Robbers model are only able to fit the distance to recombination well by changing Ω_m and H_0 from their true values. Therefore, including a strong, 1% prior on H_0 in addition to the SN, CMB, and cluster data leads to nearly unbiased constraints on the curvature for this model of early dark energy. Including the full CMB constraints instead of just the distance priors would also help in this case, since the

2% early dark energy fraction at recombination would be detectable in Planck data.

For models with massive neutrinos, the results of the growth reconstruction analysis are similar to those for early dark energy models. Massive neutrinos suppress growth on scales below their free streaming length [64, 65], affecting the growth evolution in a manner similar to dark energy that tracks the dominant matter or radiation density at early times ($w_\infty = 0$). Some of the strongest current cosmological limits on the neutrino mass come from the combination of the Lyman- α forest power spectrum with CMB data, with a 95% CL upper limit on the sum of neutrino masses of $\sum m_\nu < 0.17$ eV, assuming flat Λ CDM [66]. More conservative upper bounds limit the masses to $\sum m_\nu < 1.3$ eV (95% CL) using the CMB alone and $\sum m_\nu < 0.67$ eV (95% CL) with CMB, BAO, and SN data (also assuming flat Λ CDM [1]). On the other hand, neutrino oscillation experiments indicate that there must be at least one neutrino mass eigenstate with $m_\nu \gtrsim 0.05$ eV (e.g., [67, 68]).

Using w_∞ as an effective parameter to absorb the effects of massive neutrinos on distances and growth, the resulting curvature estimates tend to be biased toward high values of Ω_K . The bias is similar to what we found for the Doran & Robbers early dark energy model above, and as in that case an additional H_0 prior can reduce the curvature bias. Without any extra priors, the curvature can be biased by as much as $\sim 0.5\sigma$ even for the minimal mass of $\sum m_\nu \approx 0.05$ eV, so proper modeling of the effects of massive neutrinos is likely to be important for future curvature constraints from distances and growth.

Using the sum of neutrino masses as an additional parameter in the growth reconstruction analysis, instead of modeling the effects of neutrinos with w_∞ , produces unbiased curvature constraints. However, for models with massive neutrinos the uncertainty in curvature is fairly large due to a strong degeneracy between Ω_K and $\sum m_\nu$. In such a scenario, independent measurements of the neutrino masses would greatly reduce the uncertainty in curvature from distance and growth probes. Future cosmological measurements such as weak lensing of the CMB may be able to determine neutrino masses with an accuracy of $\sigma(\sum m_\nu) \approx 0.05$ eV, which should yield strong constraints on neutrino masses when combined with the results of terrestrial experiments (e.g., see [69] for a review).

For the most general treatment of the high-redshift universe, one should ideally include parameters for both massive neutrinos and early dark energy models. We leave further study of this approach for future work, but note here that a simultaneous analysis of the impact of massive neutrinos and early dark energy on curvature estimation may be complicated by degeneracies between the two in the distance and growth observables.

C. Dependence on SN and CMB data modeling

Using the growth reconstruction method, we can study the relative contributions of scatter in the SN and CMB data to uncertainties in the reconstructed growth function by only including the scatter in one of these data sets in the Monte Carlo simulations. For the predicted growth observables $P_d(\mathbf{g}|\Omega_K)$, the SN errors assumed for SNAP are the dominant source of uncertainty. More precise CMB data than anticipated from Planck would have little impact on the uncertainties in the growth reconstruction. However, for the *curvature* constraint, more precise SN or CMB data would not significantly reduce $\sigma(\Omega_K)$ since the assumed 1% growth uncertainties for IXO clusters dominate the curvature uncertainty.

If we could obtain more precise growth measurements with uncertainties less than a few tenths of a percent, then the curvature estimate would be limited by the precision of the data from SNAP and Planck. However, the relative importance of these two data sets for curvature is opposite that for $P_d(\mathbf{g}|\Omega_K)$. That is, given extremely precise growth measurements, $\sigma(\Omega_K)$ would be reduced more by improving CMB data beyond Planck than by reducing SN uncertainties. The reason for this is related to the covariance between $G_0(z)$ and $G(z_{\max})$: as explained above (see Fig. 9), CMB data induce a positive correlation between the reconstructions of $G_0(z)$ and $G(z_{\max})$ from distance data. Since changing the curvature has opposite effects on $G_0(z)$ and $G(z_{\max})$, the covariance from CMB constraints leads to more precise limits on curvature. Improving CMB constraints therefore reduces curvature uncertainty by strengthening the $G_0(z) - G(z_{\max})$ correlation.

The curvature forecasts are not strongly dependent on the redshift distribution of the supernova sample. For example, if we assume a uniform distribution of 2300 SNe over $0 < z < 1.7$ instead of the SNAP distribution of 2000 SNe plus 300 low- z SNe, the curvature estimate from SNAP+Planck+IXO is unchanged.

Interpolation of the distance–redshift relation between redshift bins or across gaps in the SN data introduces additional assumptions about the evolution of the expansion rate. To test the impact of these assumptions, we have tried several distinct methods for interpolating between bins and found that the reconstructed growth changes by $\lesssim 1\%$, and the mean value of Ω_K in forecasts changes by $\lesssim 5 \times 10^{-4}$. However, there is always an inherent assumption about smoothness of $\chi(z)$ in the growth reconstruction method that should be kept in mind when interpreting the results.

D. Dependence on cluster data modeling

We have assumed fairly optimistic future growth constraints for the curvature forecasts, with 1% measurements of the growth function at $z < 1.5$ as anticipated for the proposed IXO cluster sample [51]. We can eas-

ily study how the curvature forecasts depend on the assumed precision of the growth measurements by rescaling the Fisher matrix of the growth observables \mathbf{F}_g used in Eq. (31). We find that for less optimistic assumptions about the growth uncertainties, it is still possible to obtain interesting model-independent estimates of the curvature. For example, doubling the growth uncertainties to 2% increases the curvature uncertainty from $\sigma(\Omega_K) = 0.0022$ to $\sigma(\Omega_K) = 0.0033$, and for 3% growth measurements, $\sigma(\Omega_K) = 0.0045$.

The forecasts presented in the previous sections assume that the cluster likelihood can be approximated as a multivariate Gaussian distribution for uncorrelated growth observables $\{G_0(z_i)\}$ in $\Delta z = 0.1$ redshift bins and $G(z_{\max})$. In reality, we can expect that at least some of the growth observables will be correlated. Perhaps more importantly, the observed cluster abundance depends on distances and the expansion rate as well as the growth function, and there may be degeneracies between these functions in the cluster likelihood. We might expect that the effect on curvature estimates of treating cluster abundance as purely a probe of the growth history is small since the distance–redshift relation is well constrained by the SN and CMB data. Although a detailed study of curvature constraints using the full cluster likelihood is beyond the scope of this work, we present a simple test of this expectation here.

To check how well the fiducial distance data sets constrain degeneracies between distances and growth in the cluster likelihood, we compute the Fisher matrix for growth and distance assuming Poisson-distributed clusters [70, 71],

$$F_{\alpha\beta} = \sum_{i,j} \frac{1}{N(M_i, z_j)} \frac{\partial N(M_i, z_j)}{\partial \theta_\alpha} \frac{\partial N(M_i, z_j)}{\partial \theta_\beta}, \quad (34)$$

where $\boldsymbol{\theta} = (\{G_0(z_j)\}, \{H_0 D(z_j)\})$, taking derivatives of the number of clusters in each bin $N(M_i, z_j)$ at the fiducial flat Λ CDM model. The mass bins $\{M_i\}$ have width $\Delta \ln M \approx 0.35$ and start at a mass threshold M_{\min} , and the redshift bins $\{z_j\}$ have width $\Delta z = 0.1$ and cover the range $0.1 \leq z \leq 1.5$.

As described in Sec. II C, the abundance of massive clusters is exponentially sensitive to growth through the mass function dn/dM [Eq. (9)]. However, the observed number of clusters depends on the cosmological model in other ways as well. In particular, the comoving volume element [Eq. (8)] introduces additional dependence on the distance–redshift relation and expansion rate. The mass dependence of the effective volume in which a given survey probes clusters of a certain mass is also cosmology-dependent (and redshift-dependent) in general, although here for simplicity we take the volume to be constant above a mass threshold $M_{\min} = 10^{14} h^{-1} M_\odot$.

The main mass proxy proposed for IXO is the product of the X-ray temperature T_X and gas mass M_{gas} , $Y_X = T_X M_{\text{gas}}$, which is expected to have a relatively small, $< 10\%$ scatter based on cluster simulations [72].

Assuming lognormal scatter in the $Y_X - M$ relation, the total number of clusters in redshift bin z_j with width Δz and mass bin $M_i < M < M_{i+1}$ is [73]

$$N(M_i, z_j) \approx \frac{\Delta z}{2} \int_{-\infty}^{\infty} d \ln M \frac{dn(M, z_j)}{d \ln M} \frac{dV(z_j)}{d\Omega dz} \quad (35)$$

$$\times \left[\operatorname{erf} \left(\frac{\ln M_{i+1} - \ln M}{\sqrt{2} \sigma_{\ln M}} \right) - \operatorname{erf} \left(\frac{\ln M_i - \ln M}{\sqrt{2} \sigma_{\ln M}} \right) \right].$$

We include a 3% systematic error in M in uncorrelated $\Delta z = 0.1$ redshift bins to represent the IXO forecast for the error in the normalization of the $Y_X - M$ relation from weak lensing mass measurements of 100 clusters per redshift bin [73].

Cluster mass estimates generally also depend on the assumed cosmology, although the exact dependence varies for different mass proxies. Recent results from simulations indicate that this additional cosmological dependence is fairly weak [74], but it is nevertheless important to include in a full analysis of cluster data. For simplicity, however, we neglect the cosmological dependence of the cluster masses here and assume that the sensitivity of cluster abundances to cosmology is dominated by the mass function and the volume element.

For the halo mass function [Eq. (9)], we use the parametrization fit to simulations in Ref. [75],

$$f(\sigma) = A(z) \left[\left(\frac{\sigma}{b(z)} \right)^{-a(z)} + 1 \right] e^{-c/\sigma^2}, \quad (36)$$

where A , a , and b are weakly redshift-dependent. As the authors of that paper note, it is probably more appropriate for the wide variety of cosmological models considered here to replace the redshift dependence of these parameters with dependence on the growth function. In fact, it may be important to include dependence on not only the instantaneous value of the growth function at the redshift of a cluster, but also the evolution of the growth function prior to that redshift [76]. Recent studies using N-body simulations or semi-analytic modeling of nonlinear growth in cosmologies with more complex dark energy evolution than Λ CDM have begun to examine such issues [77, 78, 79, 80, 81, 82, 83, 84, 85, 86]. For the approximate modeling of the cluster mass function here, however, we use the simpler redshift dependence given by Ref. [75].

By taking the submatrix of $F_{\alpha\beta}$ from Eq. (34) that corresponds to $\{G_0(z_j)\}$ only and inverting to get the covariance matrix, we find that the growth uncertainties for *fixed* distances are $\sim 1\%$. Marginalizing over the distances by inverting the full Fisher matrix, including both growth and distance variables, increases the growth function uncertainties by a factor of 5 – 10. However, adding SNAP-like SN distance constraints with 1% accuracy in $\{H_0 D(z_i)\}$ reduces the growth uncertainties after marginalizing over distances to 1 – 3%. Recall from the beginning of this section that 3% growth function uncertainties approximately double the error in the curvature estimate relative to 1% growth uncertainties.

This test shows that distances at low z should be constrained well enough by the future SN and CMB data that the impact of additional cluster data can be roughly approximated by its expected accuracy on the growth function alone. Including degeneracies between growth and distances in the halo mass function and comoving volume element results in somewhat weaker but still interesting constraints on curvature. However, given the simplifying assumptions made here, curvature constraints from distance and growth data using the full cluster likelihood are a subject that deserves further exploration.

E. Comparison with other methods

The model-independent curvature constraint from distances and growth has a forecasted accuracy of $\sigma(\Omega_K) = 0.002$ for SNAP SN, Planck CMB, and IXO cluster data, assuming that the true cosmology is close to flat Λ CDM. This is very close to the accuracy expected in the model-dependent context of Λ CDM using the SN and CMB distance data only. Thus the inclusion of growth information provides a curvature measurement that is free from possible biases due to assuming an incorrect form of the dark energy evolution without sacrificing precision.

As we have seen, other types of measurements can play a similar role to the growth constraints. A 1% measurement of the Hubble constant and a 1% upper limit on the fraction of dark energy at recombination, when combined with SNAP SN and Planck CMB data, provide a model-independent curvature constraint with $\sigma(\Omega_K) \sim 0.005$. However, this constraint is strongly skewed with a long tail toward open models, and without growth information the constraints such data can place on cosmologies that have significant amounts of early dark energy are severely limited.

The method of curvature estimation studied here can provide complementary constraints to other model-independent techniques. Knox [19] proposed using precise distance measurements, for example from BAO at high redshifts ($z \gtrsim 3$), in comparison with the distance to recombination measured in CMB data to probe curvature. With future, percent-level BAO distances and Planck CMB data, this method is expected to attain an accuracy of $\sigma(\Omega_K) \sim 0.001 - 0.002$ [19, 87, 88]. However, this measurement depends on the assumption that the universe is matter-dominated between the redshift of the BAO measurement and recombination. As a result, the estimated curvature is independent of the low-redshift dark energy modeling but still depends on the high-redshift dark energy evolution [19]. This dependence is similar to the degeneracy between curvature and early dark energy that we find when comparing high- z SN distances to the CMB distance [Eq. (18)]. Additional information, such as a measurement of $G(z)$ (or σ_8), or BAO in the line-of-sight direction to probe $H(z)$ at $z \sim 3$, could help to reduce the high- z model dependence of this

method [19].

The curvature measurement proposed by Bernstein [18] is perhaps the most model-independent method since it relies only on the FRW form of the metric without assuming particular dark energy properties and is valid for alternative theories of gravity as well. Weak lensing galaxy-shear correlations can measure distance “triangles” involving the lens distance, source distance, and the distance between the two, and the relations between these distances are sensitive to curvature. Future lensing and galaxy surveys can provide a purely geometric test of curvature with an expected accuracy of $\sigma(\Omega_K) \sim 0.02 - 0.04$ [18, 89]. This technique is likely to be even less model-dependent than the distance plus growth method described here, but the forecasted uncertainties are an order of magnitude larger.

Given that each of these methods for obtaining model-independent curvature estimates relies on different types of data, it is difficult to compare forecasts directly. On the other hand, the existence of multiple methods using independent data sets means that there will be many opportunities for cross-checks of the curvature estimates. In this sense, it is useful to have an array of model-independent methods available that will have different systematics, both theoretical and instrumental.

VII. DISCUSSION

With future supernova and CMB data sets making definite predictions for the growth of linear perturbations based on measured distances, precise measurements of the actual growth history will provide model-independent estimates of spatial curvature. Such constraints have important implications for testing models of inflation, which predict $\Omega_K \approx 0$, and for obtaining constraints on dark energy models that are robust to uncertainty in curvature.

If the true cosmology is similar to flat Λ CDM, as current data would suggest, then a combination of SNe from SNAP, CMB data from Planck, and X-ray clusters from IXO can measure the curvature with an accuracy of $\sigma(\Omega_K) \approx 0.002$, making minimal assumptions about the dark energy evolution. The main constraint on curvature in this scenario comes from combining distance data with measurements of the evolution of the growth function at low redshifts. However, information about the normalization of growth relative to early times, obtained by comparing cluster abundances with the amplitude of CMB anisotropies, can significantly reduce the uncertainty in curvature. The extra information mainly comes from the covariance between the growth normalization and the low-redshift growth evolution required by the CMB constraint on the distance to recombination.

These forecasts are robust to changes in the true value of the curvature and in the dark energy evolution at low redshift. However, if the true cosmology is significantly different from the concordance flat Λ CDM model at high

redshifts ($z \gtrsim 2$), then the forecasted errors on Ω_K increase by a factor of a few and the constraints depend more strongly on the normalization of the low-redshift growth function relative to early times. Although model-independent limits on curvature alone are weaker in this scenario, the combination of future SN, CMB, and cluster data would reduce the allowed model space to a narrow degeneracy between curvature and early dark energy or massive neutrinos. A precise independent measurement of the Hubble constant would mitigate possible biases in these constraints.

Estimates of curvature from distances and growth are complementary to other model-independent techniques. The projected accuracy is similar to that expected from comparing distances measured at $z \sim 3$ to the distance to recombination [19], but the inclusion of growth information reduces dependence on assumptions about the high-redshift universe. Compared with proposed metric tests of curvature using weak lensing distance triangles [18], constraints from distances and growth are more model-dependent, in particular relying on the assumption that GR is valid on large scales and that dark energy clustering does not significantly affect the growth observables. However, limits on curvature from combinations of distance and growth data are potentially much more precise.

We have focused here on the use of X-ray clusters to probe the growth history, but there are a number of other possible methods for measuring growth that may also provide interesting curvature constraints when combined with distance measurements. Correlations involving weak lensing shear and galaxy density measurements should constrain both distances and growth in several redshift bins (e.g., [89]). Redshift space distortions of galaxy correlation functions can be used to constrain the growth rate rather than the integrated growth, so such data sets may provide interesting complementary constraints to those from clusters or weak lensing. Forecasts of the ability of these alternative probes of growth to measure curvature when combined with distance data are an interesting subject for future study.

A fundamental assumption for using distances and growth to measure spatial curvature is that the relation between the growth history and the expansion rate is governed by GR. In the context of modified theories of gravity, many authors have studied the use of distances and growth to test for deviations from GR. These investigations typically make some simplifying assumptions regarding spatial flatness and/or the dark energy evolution, and relaxing these assumptions could make such tests of gravity considerably more complicated. For example, at any particular scale the deviations in the distance-growth relation caused by modifying gravity may be difficult to distinguish from the effects of nonzero curvature or dynamical dark energy. However, scale dependence of growth could still be a robust signature of certain classes of modified gravity theories even in the context of more general cosmologies. Regardless of our ability to use future data to distinguish between nonzero curvature, dy-

namical dark energy, and modified gravity, finding hints of any of these possibilities would be an intriguing sign of physics beyond the standard cosmological model.

Acknowledgments: The author would like to thank Wayne Hu, Cora Dvorkin, and Amol Upadhye for useful discussions. This work was supported by the NSF GRFP.

APPENDIX A: GROWTH FUNCTION APPROXIMATION AT HIGH REDSHIFT

At high redshift, assuming that the contributions of dark energy and curvature to $H(z)$ are much smaller than that of the matter density, we can derive an approximate form for the growth history. In an Einstein-de Sitter universe with matter only, the growth function is constant. We therefore start with an *ansatz* that the growth history in a universe with small fractions of dark energy and curvature is a small perturbation to the constant Einstein-de Sitter solution, expanding around some redshift z_i where $G(z_i) = G_i$,

$$G(z) = G_i + C_{\text{EDE}} \left[\left(\frac{1+z}{1+z_i} \right)^{3w_\infty} - 1 \right] + C_{\text{curv}} \left[\left(\frac{1+z}{1+z_i} \right)^{-1} - 1 \right], \quad (\text{A1})$$

where $C_{\text{EDE}} \ll G_i$, $C_{\text{curv}} \ll G_i$, and we have assumed that dark energy at early times can be parametrized by a constant effective equation of state w_∞ . The redshift dependence of the terms in Eq. (A1) is the same as that of $\Omega_{\text{DE}}(z)$ and $\Omega_K(z)$ during matter domination. The growth solution must have this dependence in order to solve Eq. (6) since $d \ln H / d \ln a$ contains terms proportional to $\Omega_{\text{DE}}(z)$ and $\Omega_K(z)$.

For this approximate solution to the growth equation, we neglect terms of second or higher order in C_{EDE} , C_{curv} , $\Omega_{\text{DE}}(z_i)$, and $\Omega_K(z_i)$. In this limit, the quantity $d \ln H / d \ln a$ appearing in Eq. (6) is

$$\frac{d \ln H}{d \ln a} \approx -\frac{3}{2} + \frac{1}{2} \Omega_K(z) - \frac{3}{2} w_\infty \Omega_{\text{DE}}(z). \quad (\text{A2})$$

Using Eqs. (A1) and (A2) in the differential equation for $G(z)$ produces algebraic relations for the early dark energy and curvature coefficients:

$$C_{\text{EDE}} = \frac{1 - w_\infty}{w_\infty(5 - 6w_\infty)} \Omega_{\text{DE}}(z_i) G_i, \quad (\text{A3})$$

$$C_{\text{curv}} = -\frac{4}{7} \Omega_K(z_i) G_i. \quad (\text{A4})$$

This approximation can be used to set the value of $\delta'(z_{\max})$ needed for the analytic growth reconstruction in Sec. V:

$$\begin{aligned} \delta'(z_{\max}) &= -\frac{\delta(z_{\max})}{(1+z_{\max})} \frac{H(z_{\max})}{H_0} \\ &\quad \times \left(1 + \frac{d \ln G}{d \ln a} \Big|_{z_{\max}} \right), \quad (\text{A5}) \\ \frac{d \ln G}{d \ln a} \Big|_{z_{\max}} &= -\frac{3(1-w_\infty)}{5-6w_\infty} \Omega_{\text{DE}}(z_{\max}) - \frac{4}{7} \Omega_{\text{K}}(z_{\max}). \end{aligned}$$

The approximation breaks down when either the curvature or early dark energy fraction is large. For $\Omega_{\text{DE}}(z_{\max}) < 0.25$ and $|\Omega_{\text{K}}| < 0.01$, the error in the approximation for δ'/δ at $z_{\max} \approx 1.5$ is $\lesssim 1\%$. The approximate form of the growth rate in Eq. (A5) remains accurate even as $w_\infty \rightarrow 0$ despite the fact that the integrated growth function [Eq. (A1)] becomes inaccurate at $w_\infty \gtrsim -1$.

APPENDIX B: MONTE CARLO SIMULATIONS OF GROWTH RECONSTRUCTION

The procedure we use to estimate the covariance of growth reconstructed from distances (Sec. V) for future SN and CMB data is as follows:

1. Define redshift bins $\{z_i\}$, $i = 1, \dots, n_z$ with $z_1 = 0$ and $z_{n_z} = z_{\max}$.
2. Choose the assumed values of Ω_{K} and early dark energy/massive neutrino parameters (here, we use w_∞ as an example).
3. Draw a realization of the SN data, specified by the redshift distribution of Type Ia SNe and their magnitude errors:

$$\begin{aligned} \chi_\alpha &= \frac{1}{\sqrt{|\Omega_{\text{K}}|}} S_K^{-1} \left[\sqrt{|\Omega_{\text{K}}|} (H_0 D(z_\alpha) + \epsilon_\alpha) \right], \quad (\text{B1}) \\ \epsilon_\alpha &= \epsilon_{\text{stat},\alpha} + \epsilon_{\text{sys}}(z_\alpha), \end{aligned}$$

where the statistical error $\epsilon_{\text{stat},\alpha}$ is drawn for each SN (labeled by α) from a Gaussian with width $\sigma_{H_0 D, \alpha} = 0.15 H_0 D(z_\alpha) / (5 \log e)$, and the systematic error $\epsilon_{\text{sys}}(z_\alpha)$ is drawn for each $\Delta z = 0.1$ redshift bin from a Gaussian with width $0.02[(1+z)/2.7]/(5 \log e)$. The SN distance–redshift relation is assumed to be unbiased relative to the fiducial model for the data, so $\langle \epsilon_\alpha \rangle = 0$.

4. Estimate $z(\chi)$ from the SN data by first estimating $\chi(z)$ and then inverting the relation. We compute $\chi(z)$ in redshift bins z_i with width Δz as

$$\chi(z_i) = \frac{\sum_\alpha \chi_\alpha \exp[-(z_\alpha - z_i)^2 / (2\Delta z^2)]}{\sum_\alpha \exp[-(z_\alpha - z_i)^2 / (2\Delta z^2)]}, \quad (\text{B2})$$

where z_α and χ_α are the redshifts and χ values of SNe from step 3. The default bin width used here is $\Delta z = 0.05$.

To invert this to obtain $z(\chi)$, the estimated $\chi(z_i)$ must be monotonic. For large enough Δz this is typically not a problem since the fiducial $\chi(z)$ relation is always monotonically increasing, but even with wide redshift bins there is a chance of having a few realizations with non-monotonic $\chi(z_i)$ estimates. We correct for this when it occurs by simply setting $\chi(z_{i+1}) = \chi(z_i)$ in any bin for which Eq. (B2) gives $\chi(z_{i+1}) < \chi(z_i)$. The fact that the results are relatively independent of the redshift bin width indicates that this correction is not a significant source of error.

SN coverage that is fairly uniform in z is important to avoid bias in the $z(\chi)$ relation. For the anticipated SNAP distribution the largest biases are at the ends, $z \approx 0$ and $z \approx z_{\max}$. The low- z bias has little impact on the growth reconstruction at $z \gtrsim 0.1$, but the high- z bias can cause problems with connecting the reconstructed growth at $z < z_{\max}$ to the fiducial $z > z_{\max}$ growth history. To avoid such problems, we take z_{\max} for the growth reconstruction to be slightly smaller than the maximum SN redshift; in the case of SNAP where the SN distribution ends at $z = 1.7$, $z_{\max} = 1.5$ is sufficiently low to avoid problems relating to bias in $z(\chi)$. (Note that using a different value of z_{\max} results in slightly different definitions of early dark energy for the MCMC and growth reconstruction methods.)

5. Estimate $E_{\max} = dz/d\chi(z_{\max})$ using a linear fit to the high- z end of the $z(\chi)$ relation.
6. Draw simulated CMB distance data from the 2×2 Fisher matrix for $\{\ln(D_*/\text{Mpc}), \Omega_{\text{m}} h^2\}$ (Sec. II E). Using the assumed curvature and early dark energy parameters in addition to the estimate of E_{\max} from step 5, set Ω_{m} and h to match the CMB constraints.
7. Optionally include additional priors (e.g. H_0 and dark energy fraction at last scattering). Each Monte Carlo simulation is weighted by the likelihood associated with these priors, and the entire set of simulations for a single $\{\Omega_{\text{K}}, w_\infty\}$ pair has a weight assigned to it equal to the average of the individual simulation weights.
8. Compute the growth at z_{\max} relative to recombination, $G(z_{\max})$, for the expansion history specified by Ω_{K} and w_∞ (step 2); E_{\max} (step 5); and Ω_{m} and h (step 6).
9. Given $z(\chi)$ from step 4 and Ω_{m} from step 5, iteratively solve the growth reconstruction equation, Eq. (27). For each iteration, δ'_{\max} is set to the average of its value in the previous iteration and the target value based on the approximate growth evolution at $z > z_{\max}$ given by Eq. (A5).

10. Repeat steps 3 – 9 for many realizations of the SN and CMB data, and compute the mean and covariance (using the weights from step 7) of the resulting estimates of $\mathbf{g} = \{G(z_{\max}), G_0(z_i)\}$. This produces the predicted growth observables at fixed Ω_K and w_∞ .
11. Repeat steps 2 – 10 for different curvature and early dark energy parameter values to compute $P_d(\mathbf{g}|\Omega_K, w_\infty)$.

-
- [1] E. Komatsu, J. Dunkley, M. R. Nolta, C. L. Bennett, B. Gold, G. Hinshaw, N. Jarosik, D. Larson, M. Limon, L. Page, et al., *Astrophys. J. Suppl.* **180**, 330 (2009), arXiv:0803.0547.
- [2] D. J. Eisenstein, I. Zehavi, D. W. Hogg, R. Scoccimarro, M. R. Blanton, R. C. Nichol, R. Scranton, H.-J. Seo, M. Tegmark, Z. Zheng, et al., *Astrophys. J.* **633**, 560 (2005), arXiv:astro-ph/0501171.
- [3] G.-B. Zhao, J.-Q. Xia, H. Li, C. Tao, J.-M. Virey, Z.-H. Zhu, and X. Zhang, *Physics Letters B* **648**, 8 (2007), arXiv:astro-ph/0612728.
- [4] K. Ichikawa and T. Takahashi, *Journal of Cosmology and Astro-Particle Physics* **2**, 1 (2007), arXiv:astro-ph/0612739.
- [5] E. L. Wright, *Astrophys. J.* **664**, 633 (2007), arXiv:astro-ph/0701584.
- [6] S. Weinberg, *Astrophys. J. Lett.* **161**, L233 (1970).
- [7] J. R. Bond, G. Efstathiou, and M. Tegmark, *Mon. Not. R. Astron. Soc.* **291**, L33 (1997), arXiv:astro-ph/9702100.
- [8] M. Zaldarriaga, D. N. Spergel, and U. Seljak, *Astrophys. J.* **488**, 1 (1997), arXiv:astro-ph/9702157.
- [9] G. Efstathiou and J. R. Bond, *Mon. Not. R. Astron. Soc.* **304**, 75 (1999), arXiv:astro-ph/9807103.
- [10] G. Huey, L. Wang, R. Dave, R. R. Caldwell, and P. J. Steinhardt, *Phys. Rev. D* **59**, 063005 (1999), arXiv:astro-ph/9804285.
- [11] E. V. Linder, *Astroparticle Physics* **24**, 391 (2005), arXiv:astro-ph/0508333.
- [12] D. Polarski and A. Ranquet, *Physics Letters B* **627**, 1 (2005), arXiv:astro-ph/0507290.
- [13] C. Clarkson, M. Cortès, and B. Bassett, *Journal of Cosmology and Astro-Particle Physics* **8**, 11 (2007), arXiv:astro-ph/0702670.
- [14] J.-M. Virey, D. Talon-Esmieu, A. Ealet, P. Taxil, and A. Tilquin, *Journal of Cosmology and Astro-Particle Physics* **12**, 8 (2008), arXiv:0802.4407.
- [15] R. Hlozek, M. Cortès, C. Clarkson, and B. Bassett, *General Relativity and Gravitation* **40**, 285 (2008), arXiv:0801.3847.
- [16] Z.-Y. Huang, B. Wang, and R.-K. Su, *International Journal of Modern Physics A* **22**, 1819 (2007), arXiv:astro-ph/0605392.
- [17] R. R. Caldwell and M. Kamionkowski, *Journal of Cosmology and Astro-Particle Physics* **9**, 9 (2004), arXiv:astro-ph/0403003.
- [18] G. Bernstein, *Astrophys. J.* **637**, 598 (2006), arXiv:astro-ph/0503276.
- [19] L. Knox, *Phys. Rev. D* **73**, 023503 (2006), arXiv:astro-ph/0503405.
- [20] W. Hu, in *Observing Dark Energy*, edited by S. C. Wolff and T. R. Lauer (2005), vol. 339 of *Astronomical Society of the Pacific Conference Series*, p. 215, arXiv:astro-ph/0407158.
- [21] W. Hu, D. Huterer, and K. M. Smith, *Astrophys. J. Lett.* **650**, L13 (2006), arXiv:astro-ph/0607316.
- [22] M. J. Mortonson, W. Hu, and D. Huterer, *Phys. Rev. D* **79**, 023004 (2009), arXiv:0810.1744.
- [23] U. Alam, V. Sahni, and A. A. Starobinsky (2008), arXiv:0812.2846.
- [24] A. Kashlinsky, I. I. Tkachev, and J. Frieman, *Physical Review Letters* **73**, 1582 (1994), arXiv:astro-ph/9405024.
- [25] M. Bucher, A. S. Goldhaber, and N. Turok, *Phys. Rev. D* **52**, 3314 (1995), arXiv:hep-ph/9411206.
- [26] T. P. Waterhouse and J. P. Zibin (2008), arXiv:0804.1771.
- [27] M. Vardanyan, R. Trotta, and J. Silk, *Mon. Not. R. Astron. Soc.* p. 812 (2009), arXiv:0901.3354.
- [28] J. R. Gott, III, *Nature (London)* **295**, 304 (1982).
- [29] G. F. R. Ellis, D. H. Lyth, and M. B. Mijić, *Physics Letters B* **271**, 52 (1991).
- [30] M. Sasaki, T. Tanaka, K. Yamamoto, and J. Yokoyama, *Physics Letters B* **317**, 510 (1993).
- [31] A. Linde and A. Mezhlumian, *Phys. Rev. D* **52**, 6789 (1995), arXiv:astro-ph/9506017.
- [32] S. W. Hawking and N. Turok, *Physics Letters B* **425**, 25 (1998), arXiv:hep-th/9802030.
- [33] S. Gratton, A. Lewis, and N. Turok, *Phys. Rev. D* **65**, 043513 (2002), arXiv:astro-ph/0111012.
- [34] J.-P. Uzan, U. Kirchner, and G. F. R. Ellis, *Mon. Not. R. Astron. Soc.* **344**, L65 (2003), arXiv:astro-ph/0302597.
- [35] A. Linde, *Journal of Cosmology and Astro-Particle Physics* **5**, 2 (2003), arXiv:astro-ph/0303245.
- [36] A. Lasenby and C. Doran, *Phys. Rev. D* **71**, 063502 (2005), arXiv:astro-ph/0307311.
- [37] B. Freivogel, M. Kleban, M. Rodríguez Martínez, and L. Susskind, *Journal of High Energy Physics* **3**, 39 (2006), arXiv:hep-th/0505232.
- [38] D. N. Spergel, L. Verde, H. V. Peiris, E. Komatsu, M. R. Nolta, C. L. Bennett, M. Halpern, G. Hinshaw, N. Jarosik, A. Kogut, et al., *Astrophys. J. Suppl.* **148**, 175 (2003), arXiv:astro-ph/0302209.
- [39] E. Rozo, R. H. Wechsler, E. S. Rykoff, J. T. Annis, M. R. Becker, A. E. Evrard, J. A. Frieman, S. M. Hansen, J. Hao, D. E. Johnston, et al. (2009), arXiv:0902.3702.
- [40] A. Vikhlinin, A. V. Kravtsov, R. A. Burenin, H. Ebeling, W. R. Forman, A. Hornstrup, C. Jones, S. S. Murray, D. Nagai, H. Quintana, et al., *Astrophys. J.* **692**, 1060 (2009), arXiv:0812.2720.
- [41] B. Ratra and P. J. E. Peebles, *Phys. Rev. D* **37**, 3406 (1988).
- [42] P. G. Ferreira and M. Joyce, *Phys. Rev. D* **58**, 023503 (1998), arXiv:astro-ph/9711102.
- [43] P. J. Steinhardt, L.-M. Wang, and I. Zlatev, *Phys. Rev. D* **59**, 123504 (1999), arXiv:astro-ph/9812313.
- [44] G. Aldering et al. (2004), arXiv:astro-ph/0405232.
- [45] The Planck Collaboration (2006), arXiv:astro-ph/0604069.

- [46] W. L. Freedman, B. F. Madore, B. K. Gibson, L. Ferrarese, D. D. Kelson, S. Sakai, J. R. Mould, R. C. Kennicutt, Jr., H. C. Ford, J. A. Graham, et al., *Astrophys. J.* **553**, 47 (2001), arXiv:astro-ph/0012376.
- [47] M. Doran, G. Robbers, and C. Wetterich, *Phys. Rev. D* **75**, 023003 (2007), arXiv:astro-ph/0609814.
- [48] L. Greenhill et al. (2009), arXiv:0902.4255.
- [49] R. de Putter, O. Zahn, and E. V. Linder, *Phys. Rev. D* **79**, 065033 (2009), arXiv:0901.0916.
- [50] L. Hollenstein, D. Sapone, R. Crittenden, and B. M. Schäfer, *Journal of Cosmology and Astro-Particle Physics* **4**, 12 (2009), arXiv:0902.1494.
- [51] A. Vikhlinin, S. W. Allen, M. Arnaud, M. Bautz, H. Boehringer, M. Bonamente, J. Burns, A. Evrard, J. P. Henry, C. Jones, et al. (2009), arXiv:0903.2297.
- [52] O. Zahn and M. Zaldarriaga, *Phys. Rev. D* **67**, 063002 (2003), arXiv:astro-ph/0212360.
- [53] M. J. Mortonson and W. Hu, *Astrophys. J.* **672**, 737 (2008), arXiv:0705.1132.
- [54] N. Christensen, R. Meyer, L. Knox, and B. Luey, *Class. Quant. Grav.* **18**, 2677 (2001), arXiv:astro-ph/0103134.
- [55] A. Kosowsky, M. Milosavljevic, and R. Jimenez, *Phys. Rev. D* **66**, 063007 (2002), arXiv:astro-ph/0206014.
- [56] J. Dunkley, M. Bucher, P. G. Ferreira, K. Moodley, and C. Skordis, *Mon. Not. R. Astron. Soc.* **356**, 925 (2005), arXiv:astro-ph/0405462.
- [57] A. Gelman and D. Rubin, *Statistical Science* **7**, 452 (1992).
- [58] A. Upadhye, M. Ishak, and P. J. Steinhardt, *Phys. Rev. D* **72**, 063501 (2005), arXiv:astro-ph/0411803.
- [59] A. Lewis and S. Bridle, *Phys. Rev. D* **66**, 103511 (2002), arXiv:astro-ph/0205436.
- [60] V. Sahni and A. Starobinsky, *International Journal of Modern Physics D* **15**, 2105 (2006), arXiv:astro-ph/0610026.
- [61] M. Chevallier and D. Polarski, *International Journal of Modern Physics D* **10**, 213 (2001), arXiv:gr-qc/0009008.
- [62] E. V. Linder, *Physical Review Letters* **90**, 091301 (2003), arXiv:astro-ph/0208512.
- [63] M. Doran and G. Robbers, *Journal of Cosmology and Astro-Particle Physics* **6**, 26 (2006), arXiv:astro-ph/0601544.
- [64] J. R. Bond, G. Efstathiou, and J. Silk, *Physical Review Letters* **45**, 1980 (1980).
- [65] W. Hu and D. J. Eisenstein, *Astrophys. J.* **498**, 497 (1998), arXiv:astro-ph/9710216.
- [66] U. Seljak, A. Slosar, and P. McDonald, *Journal of Cosmology and Astro-Particle Physics* **10**, 14 (2006), arXiv:astro-ph/0604335.
- [67] D. G. Michael et al., *Physical Review Letters* **97**, 191801 (2006), arXiv:hep-ex/0607088.
- [68] T. Schwetz, M. Tórtola, and J. W. F. Valle, *New Journal of Physics* **10**, 113011 (2008), arXiv:0808.2016.
- [69] J. Lesgourgues and S. Pastor, *Physics Reports* **429**, 307 (2006), arXiv:astro-ph/0603494.
- [70] W. Cash, *Astrophys. J.* **228**, 939 (1979).
- [71] M. Tegmark, D. J. Eisenstein, W. Hu, and R. Kron (1998), arXiv:astro-ph/9805117.
- [72] A. V. Kravtsov, A. Vikhlinin, and D. Nagai, *Astrophys. J.* **650**, 128 (2006), arXiv:astro-ph/0603205.
- [73] A. Vikhlinin, R. A. Burenin, H. Ebeling, W. R. Forman, A. Hornstrup, C. Jones, A. V. Kravtsov, S. S. Murray, D. Nagai, H. Quintana, et al., *Astrophys. J.* **692**, 1033 (2009), arXiv:0805.2207.
- [74] N. Aghanim, A. C. da Silva, and N. J. Nunes, *Astron. Astrophys.* **496**, 637 (2009), arXiv:0808.0385.
- [75] J. Tinker, A. V. Kravtsov, A. Klypin, K. Abazajian, M. Warren, G. Yepes, S. Gottlöber, and D. E. Holz, *Astrophys. J.* **688**, 709 (2008), arXiv:0803.2706.
- [76] Z. Ma, *Astrophys. J.* **665**, 887 (2007), arXiv:astro-ph/0610213.
- [77] E. V. Linder and M. White, *Phys. Rev. D* **72**, 061304 (2005), arXiv:astro-ph/0508401.
- [78] M. Bartelmann, M. Doran, and C. Wetterich, *Astron. Astrophys.* **454**, 27 (2006), arXiv:astro-ph/0507257.
- [79] L. Liberato and R. Rosenfeld, *Journal of Cosmology and Astro-Particle Physics* **7**, 9 (2006), arXiv:astro-ph/0604071.
- [80] S. Basilakos and N. Voglis, *Mon. Not. R. Astron. Soc.* **374**, 269 (2007), arXiv:astro-ph/0610184.
- [81] M. J. Francis, G. F. Lewis, and E. V. Linder, *Mon. Not. R. Astron. Soc.* **380**, 1079 (2007), arXiv:0704.0312.
- [82] M. J. Francis, G. F. Lewis, and E. V. Linder, *Mon. Not. R. Astron. Soc.* **393**, L31 (2009), arXiv:0810.0039.
- [83] M. J. Francis, G. F. Lewis, and E. V. Linder, *Mon. Not. R. Astron. Soc.* **394**, 605 (2009), arXiv:0808.2840.
- [84] M. Grossi and V. Springel, *Mon. Not. R. Astron. Soc.* **394**, 1559 (2009), arXiv:0809.3404.
- [85] C. Fedeli, L. Moscardini, and M. Bartelmann, *Astron. Astrophys.* **500**, 667 (2009), arXiv:0812.1097.
- [86] L. Casarini, A. V. Macciò, and S. A. Bonometto, *Journal of Cosmology and Astro-Particle Physics* **3**, 14 (2009), arXiv:0810.0190.
- [87] L. Knox, Y.-S. Song, and H. Zhan, *Astrophys. J.* **652**, 857 (2006), arXiv:astro-ph/0605536.
- [88] G. J. Hill, K. Gebhardt, E. Komatsu, N. Drory, P. J. MacQueen, J. Adams, G. A. Blanc, R. Koehler, M. Rafal, M. M. Roth, et al., in *Astronomical Society of the Pacific Conference Series*, edited by T. Kodama, T. Yamada, and K. Aoki (2008), vol. 399 of *Astronomical Society of the Pacific Conference Series*, p. 115, arXiv:0806.0183.
- [89] H. Zhan, L. Knox, and J. A. Tyson, *Astrophys. J.* **690**, 923 (2009), arXiv:0806.0937.